Deep Sourced Fluids for Peridotite Carbonation in the Shallow Mantle Wedge of a Fossil Subduction Zone: Sr and C Isotope Profiles of OmanDP Hole BT1B

著者	de Obeso Juan Carlos, Kelemen Peter B., Leong James M., Menzel Manuel D., Manning Craig E., Godard Marguerite, Cai Yue, Bolge Louise, Oman Drilling Project Phase 1 Science Party, Usui Yoichi
著者別表示	臼井 洋一
journal or publication title	Journal of Geophysical Research: Solid Earth
volume	127
number	1
page range	e2021JB022704
year	2022-01
URL	http://doi.org/10.24517/00067023

doi: 10.1029/2021JB022704

JGR Solid Earth

RESEARCH ARTICLE
10.1029/2021JB022704

Special Section:
Ophiolites and Oceanic Lithosphere, with a focus on the Samail ophiolite in Oman

Deep Sourced Fluids for Peridotite Carbonation in the Shallow Mantle Wedge of a Fossil Subduction Zone: Sr and C Isotope Profiles of OmanDP Hole BT1B

Juan Carlos de Obeso[1,2], Peter B. Kelemen[2], James M. Leong[2], Manuel D. Menzel[3], Craig E. Manning[4], Marguerite Godard[5], Yue Cai[2], Louise Bolge[2], and Oman Drilling Project Phase 1 Science Party[6]

[1]Department of Geosciences, University of Calgary, Calgary, AB, Canada, [2]Lamont Doherty Earth Observatory, Columbia University, Palisades, NY, USA, [3]Institute of Tectonics and Geodynamics, RWTH Aachen University, Aachen, Germany, [4]Department of Earth & Space Sciences, University of California, Los Angeles, CA, USA, [5]Géosciences Montpellier, Université de Montpellier, CNRS, Montpellier, France, [6]See Appendix A

Key Points:

- Strontium and Carbon were added to the peridotites during alteration
- Strontium isotopes point to Hawasina calcite-bearing clastic sediments C as source of fluids
- Alteration fluids are derived from decarbonation reactions of subducted sediments

Supporting Information:

Supporting Information may be found in the online version of this article.

Correspondence to:

J. C. de Obeso and Y. Cai,
juancarlos.deobeso@ucalgary.ca;
merrycai@gmail.com

Citation:

de Obeso, J. C., Kelemen, P. B., Leong, J. M., Menzel, M. D., Manning, C. E., Godard, M., et al. (2022). Deep sourced fluids for peridotite carbonation in the shallow mantle wedge of a fossil subduction zone: Sr and C isotope profiles of OmanDP Hole BT1B. *Journal of Geophysical Research: Solid Earth*, *127*, e2021JB022704. https://doi.org/10.1029/2021JB022704

Received 30 JUN 2021
Accepted 16 DEC 2021

Abstract Completely carbonated peridotites represent a window to study reactions of carbon-rich fluids with mantle rocks. Here, we present details on the carbonation history of listvenites close to the basal thrust in the Samail ophiolite. We use samples from Oman Drilling Project Hole BT1B, which provides a continuous record of lithologic transitions, as well as outcrop samples from listvenites, metasediments, and metamafics below the basal thrust of the ophiolite. $^{87}Sr/^{86}Sr$ of listvenites and serpentinites, ranging from 0.7090 to 0.7145, are significantly more radiogenic than mantle values, Cretaceous seawater, and other peridotite hosted carbonates in Oman. The Hawasina sediments that underlie the ophiolite, on the other hand, show higher $^{87}Sr/^{86}Sr$ values of up to 0.7241. $\delta^{13}C$ values of total carbon in the listvenites and serpentinites range from −10.6‰ to 1.92‰. We also identified a small organic carbon component with $\delta^{13}C$ as low as −27‰. Based on these results, we propose that during subduction at temperatures above >400°C, carbon-rich fluids derived from decarbonation of the underlying sediments migrated updip and generated the radiogenic $^{87}Sr/^{86}Sr$ signature and the fractionated $\delta^{13}C$ values of the serpentinites and listvenites in core BT1B.

Plain Language Summary Samples from Oman Drilling Project Hole BT1B provide a record of interactions of fluids rich in carbon dioxide with mantle rocks. These interactions lead to the formation of listvenites, rocks composed mainly of magnesite and quartz. Here, we describe the formation of listvenites in the Oman ophiolite using Strontium and Carbon isotopes to characterize the source and nature of the fluid that pervasively transform the mantle rocks that now store vast amounts of carbon dioxide.

1. Introduction

Hydration and carbonation of ultramafic rocks are important processes in the carbon and water cycle of our planet (Alt et al., 2013; Fruh-Green et al., 2004). These alteration reactions are sinks of water and carbon where peridotites are exposed on the seafloor forming alteration minerals like serpentine and carbonates (Alt et al., 2013; Klein et al., 2020; Macdonald & Fyfe, 1985; Paulick et al., 2006) which are carried back into the mantle in convergent margins. Fluids derived from the subducted slab can migrate and interact with the mantle wedge in subduction zones, so that the "leading edge of the mantle wedge" aka the "cold nose," can be partially hydrated and carbonated (Blakely et al., 2005; Hyndman & Peacock, 2003; Kelemen & Manning, 2015). This is usually inferred from seismic data (e.g., DeShon & Schwartz, 2004; Kamiya & Kobayashi, 2000; Tibi et al., 2008; Tsuji et al., 2008). Understanding the interaction of carbon-bearing hydrous fluids with peridotites is important to supplement and constrain geophysical observations.

Fully carbonated peridotites, also known as listvenites (Halls & Zhao, 1995), provide a window into the alteration processes that occur in the "cold nose" of the mantle wedge above subduction zones, where mantle peridotite reacts with hydrous and carbonated fluids likely derived from the subducting slab at moderate temperatures and pressures (Beinlich et al., 2012; Boskabadi et al., 2017, 2020; Falk & Kelemen, 2015; Menzel et al., 2018). Formation of listvenites appears to be restricted to particular conditions requiring high carbon concentrations in the fluid (Falk & Kelemen, 2015; Hansen et al., 2005; Kelemen et al., 2021; Menzel et al., 2018). For example, complete carbonation of peridotites to form listvenites is not observed near the surface in ophiolites (e.g., Clark

& Fontes, 1990; de Obeso & Kelemen, 2018, 2020; Garcia del Real et al., 2016; Kelemen & Matter, 2008; Noël et al., 2018; Quesnel et al., 2016; Schwarzenbach et al., 2016). It is also not observed near the seafloor, where serpentinization and formation of carbonate veins are common (e.g., Bach et al., 2011; Delacour et al., 2008; Schwarzenbach et al., 2013). Fluid sources for complete carbonation have been associated with subduction in different listvenite localities. Menzel et al. (2018) attributed carbonation of harzburgite in the Advocate ophiolite (Canada) to fluxing by slab-derived, CO_2-rich fluids. Isotopic data ($\delta^{13}C$, $\delta^{18}O$, and $^{87}Sr/^{86}Sr$) of listvenites in the Late Cretaceous ophiolites of eastern Iran point to carbon-bearing fluids derived from subducted sedimentary units as the source of carbon (Boskabadi et al., 2020).

In Oman, listvenites occur along the basal thrust of the ophiolite (Nasir et al., 2007; Wilde et al., 2002). Previous studies have investigated their formation conditions and the nature of the carbonation fluids without reaching conclusive answers on the source of the fluids (Beinlich et al., 2020; Falk & Kelemen, 2015; Nasir et al., 2007; Stanger, 1985). In this study, we present $^{87}Sr/^{86}Sr$ and $\delta^{13}C$ data on samples from Oman Drilling Project Hole BT1B and the underlying sediments of the Hawasina Formation. We show that devolatization of the subducting sediments similar to the Hawasina Formation likely generated the carbonation fluids which reacted with the mantle wedge in this fossil subduction zone to form listvenites. These processes probably operate in subduction zones worldwide, where fluids migrate updip along the slab mantle interface, and then react with hanging wall peridotites storing large amounts of carbon.

2. Geological Setting

2.1. The Samail Ophiolite

The Samail ophiolite, along the northeast coast of Oman and the United Arab Emirates (UAE), is one of the best-exposed block of oceanic crust and its underlying mantle in the world. It was thrust over adjacent oceanic lithosphere soon after magmatic formation, and then onto the margin of the Arabian subcontinent in the late Cretaceous. The mantle section of the ophiolite is mainly composed of highly depleted, residual mantle peridotites (mostly harzburgites, e.g., Godard et al., 2000; Hanghøj et al., 2010; Monnier et al., 2006), together with 5%–15% dunite (Braun, 2004; Braun & Kelemen, 2002; Collier, 2012). Near the basal thrust, interlayered dunites and refertilized harzburgites comprise the distinctive "Banded Unit" (Khedr et al., 2014). The peridotites are pervasively serpentinized, with serpentine (±brucite) making up ∼ 30–100 wt% of "fresh" rock (Godard et al., 2000; Hanghøj et al., 2010; Monnier et al., 2006) and/or completely carbonated to form listvenites (Falk & Kelemen, 2015; Nasir et al., 2007; Stanger, 1985; Wilde et al., 2002). The listvenites only occur within a few km of the basal thrust of the ophiolite, and within the tectonic melanges with a serpentine matrix just below the base of the ophiolite (Nasir et al., 2007; Stanger, 1985).

2.2. Lithologies Below the Samail Ophiolite Nappe

Beneath the mantle section of the Samail ophiolite is a locally preserved "metamorphic sole." This sole is exposed discontinuously along the basal thrust, juxtaposed with the overlying Banded Unit at the base of the Samail mantle section. It records peak metamorphic temperatures of 700–900°C and imprecise peak pressures of 0.8–1.4 GPa (Cowan et al., 2014; Hacker & Mosenfelder, 1996; Searle & Cox, 2002; Searle & Malpas, 1980; Soret et al., 2017). A lower temperature unit (∼450–550°C) with similar peak pressures (0.8–1.2 GPa) has also been identified from the metamorphic section of Oman DP Hole BT1B (Kotowski et al., 2021). The base of the sole is in fault contact with low-grade allochthonous sediments of the Hawasina formation, which is composed of pelagic clastic units interlayered with limestones (Bechennec et al., 1988, 1990) deposited from the late Permian to the Cretaceous. The Hawasina sedimentary units were thrusted over autochthonous Mesozoic to Proterozoic platform sediments of the Arabian continental margin, forming nappes between the autochton and the ophiolite.

2.3. OmanDP Hole BT1B and Oman Listvenites

Hole BT1B was drilled in March 2017 in Wadi Mansah (23.364374°N, 58.182693°E), which yielded a total length of 300.1 m with 100% recovery (Kelemen et al., 2020a; Kelemen et al., 2020b). The upper 6 m are composed of alluvial gravels followed by an ultramafic sequence comprised of listvenites (carbonated peridotites) interlayered with two serpentinite bands (80–100 m depth and 181–186 m depth). A thick (0.42 m) layer of

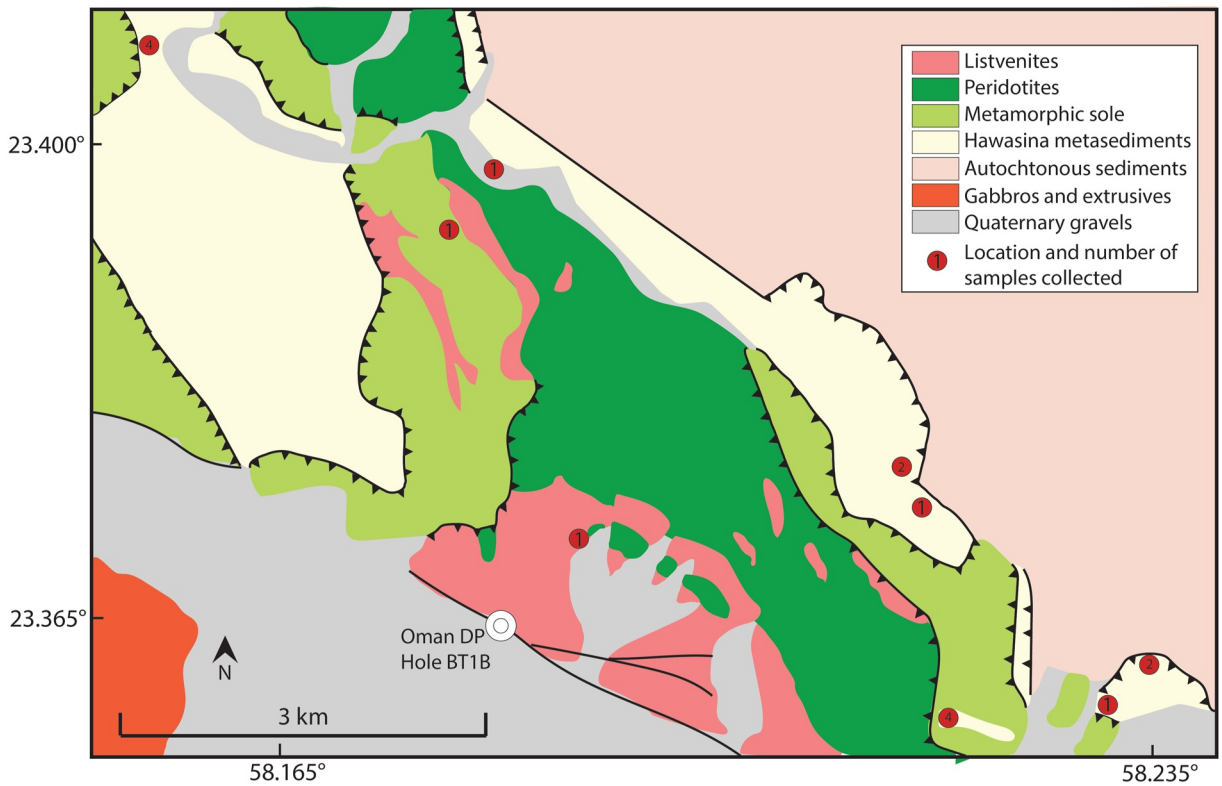

Figure 1. Simplified geologic map of Wadi Mansah and vicinity of Oman DP Hole BT1B compiled after Villey et al. (1986), Google Earth and field observations. Hand samples collected for this study are marked with red circles with number of samples collected per location in black.

gray-green fault gouge at 196.6–197.1 m depth separates the ultramafic units from the metamorphic sole composed of fine-grained metabasalts (Godard et al., 2021; Kelemen et al., 2020a; Kelemen et al., 2020b; Kelemen et al., 2021). To the first order, alteration of peridotite to form serpentinite and listvenite in Hole BT1B was nearly isochemical except for the addition of H_2O and CO_2. Average bulk rock Mg/Si, Fe/Si, Al/Si, Fe/Mg, and Cr/Al ratios in serpentinite and listvenite are close to the average composition of the Samail peridotite (Godard et al., 2021; Kelemen et al., 2020a; Kelemen et al., 2020b; Kelemen et al., 2021) and similar to the composition of previously studied listvenites from the outcrops extending north and northeast from the drill site (Falk & Kelemen, 2015). The core provides a unique record of the interaction between peridotites in the leading edge of the mantle wedge and hydrous fluids rich in CO_2. For an expanded version of the geology of Oman DP Hole BT1B and MoD mountain, we refer the reader to the Proceedings of the Oman Drilling Project (Kelemen et al., 2020a; Kelemen et al., 2020b) and Kelemen et al. (2021).

3. Materials and Methods

Samples analyzed for this study comprise a suite of drill core samples from OmanDP Hole BT1B (listvenites $n = 50$, serpentinites $n = 14$, metamorphic sole rocks $n = 11$) and hand samples of the Hawasina formation ($n = 18$) and metamorphic sole sediments ($n = 2$). Location of Oman DP Hole BT1B and Hawasina samples are shown in Figure 1. Drill core samples encompass all the identified lithologies from Hole BT1B. Major element compositions for Hole BT1B samples were reported in the *Proceedings of the Oman Drilling Project* (Kelemen et al., 2020a; Kelemen et al., 2020b) with the exception of samples in the 181–186 m depth interval which are reported by Godard et al. (2021). Trace element compositions of Hole BT1B samples can be found in Godard et al. (2021). Trace element compositions and loss on ignition for Hawasina formation outcrop samples were analyzed at Lamont Doherty Earth Observatory (LDEO). Rb and Sr concentrations were analyzed using a VG PlasmaQuad ExCell quadrupole ICP-MS following HNO_3-HF digestion. Major element compositions of the Hawasina samples are available in Table S1. Additional Sr isotopes were measured on samples from outcrops northeast of Hole BT1B (Falk & Kelemen, 2015).

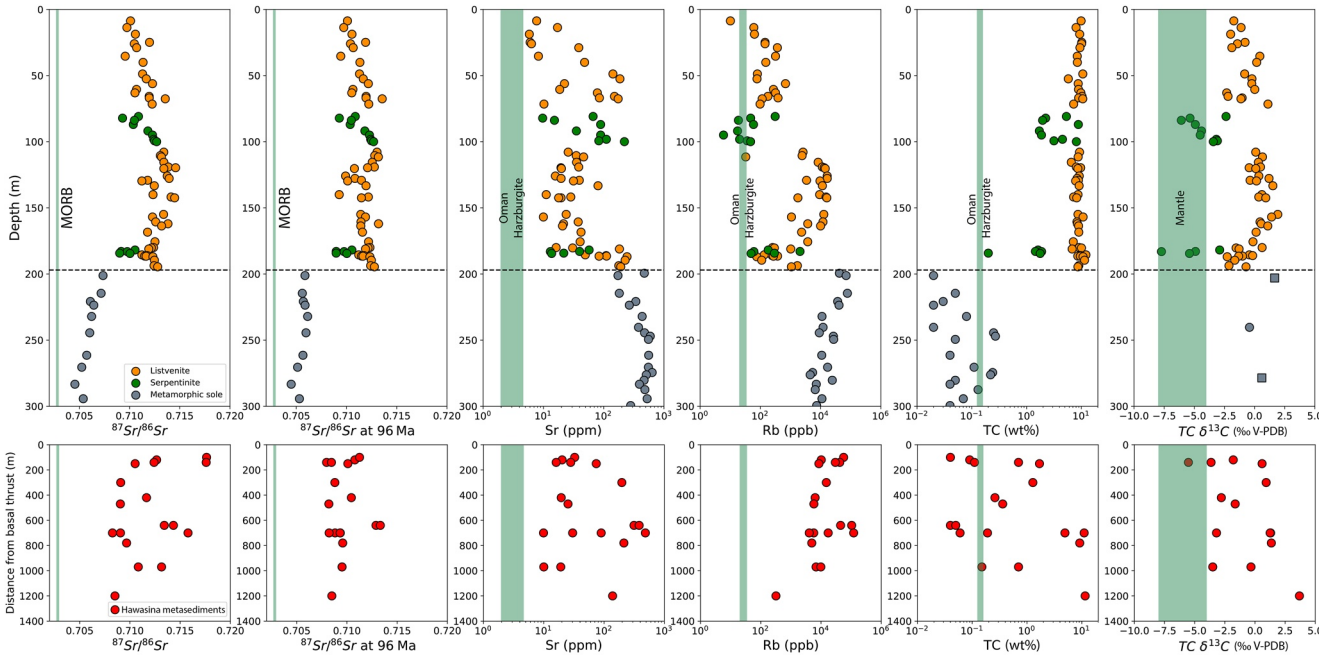

Figure 2. Depth profiles of OmanDP Hole BT1B (top panels) and distance from basal thrust for Hawasina metasediments (bottom panels). From left to right $^{87}Sr/^{86}Sr$ (measured), $^{87}Sr/^{86}$ age corrected at 96 Ma, Sr concentrations, Rb concentrations, total carbon (TC) concentration, total carbon $\delta^{13}C$ (squares in metamorphic sole from Zeko, 2021). Black dashed line in top panels correspond to basal thrust. Green reference bands in all panels indicate, from left to right: $^{87}Sr/^{86}Sr$ range of MORB (Average ± 2σ) (Gale et al., 2013; Hofmann, 2013), Sr and Rb concentration range of Oman harzburgite (Average ± 2σ) (Godard et al., 2000; Hanghøj et al., 2010; Monnier et al., 2006), total carbon content of Oman harzburgite (Average ± 2σ) (Kelemen & Manning, 2015) and mantle $\delta^{13}C$ (Average ± 2σ) (Deines, 2002). The distance from the basal thrust for the Hawasina metasediments is measured as the horizontal distance to the closest mapped metamorphic sole/ultramafic contact.

For Sr isotope analysis, bulk rock powder was fully digested in an HNO_3-HF mixture overnight and redissolved in 3N HNO_3 before column chemistry using the Eichrom® Sr resin. Purified Sr was analyzed for isotopic compositions interspersed with US National Institute of Standards and Technology (NIST) SRM 987 on a Thermo Scientific Neptune multi-collector ICP-MS at LDEO. In-run mass fractionations were normalized to $^{86}Sr/^{88}Sr = 0.1194$. Unknowns were normalized to SRM 987 $^{87}Sr/^{86}Sr$ value of 0.701248. International standards BHVO-2 yielded $^{87}Sr/^{86}Sr$ value of 0.703509 ± 41 (2σ, $n = 3$) and BCR-2 yielded 0.705046 ± 34 (2σ, $n = 3$), which agree with published values from Weis et al. (2006).

Total Carbon (TC) was measured from the same bulk rock powder splits as for Strontium isotopes. Total Organic Carbon (TOC, or reduced carbon) was measured from the residual rock powder after the removal of Inorganic Carbon (carbonate carbon) through reaction with dilute (3 N) HCl for at least 3 days, followed by washing with Millipore® water. Concentrations and $\delta^{13}C$ ratios of Total Carbon (TC) and Total Organic Carbon (TOC) were determined using a Costech element analyzer coupled with a Thermo Scientific Delta V plus mass spectrometer at LDEO. Sample runs were calibrated using Acetanilide for carbon contents ($r^2 = 0.9998$). For $\delta^{13}C$, we used USGS40 ($\delta^{13}C = -26.77 \pm 0.16$‰ V-PDB, $n = 4$), USGS41 ($\delta^{13}C = 37.63 \pm 0.12$‰ V-PDB, $n = 4$), and USGS24 ($\delta^{13}C = -16.04 \pm 0.13$‰ V-PDB, $n = 4$). All measured values of $\delta^{13}C$ standards agree with accepted values reported by the United States Geological Survey (USGS). Inorganic carbon contents and $\delta^{13}C$ of total inorganic carbon (TIC) were estimated by mass balance between TC and TOC.

4. Results

Depth profiles of $^{87}Sr/^{86}Sr$, Sr and Rb concentrations, carbon concentrations, Total Carbon, and Total carbon $\delta^{13}C$ are shown in Figure 2 and Tables 1 and 2. The Hawasina metasediments are plotted as the horizontal map distance to the closest mapped metamorphic sole/ultramafic contact.

Table 1
Lithological Information, Depth, Strontium, Rubidium, and Carbon Concentrations and Sr and C Isotope Ratios of Samples From OmanDP Hole BT1B

Sample	Depth (m)	Lithology	$^{87}Sr/^{86}Sr$	2SE total error	$^{87}Sr/^{86}Sr$ at 96 Ma	Rb (ppb)[a]	Sr (ppb)[a]	TC (wt%)	TC $\delta^{13}C$ (‰ V-PDB)	OC (wt%)	TOC $\delta^{13}C$ (‰ V-PDB)
C5704 B-7Z-4-1, 14.0–19.0 cm	8.64	Listvenite	0.710103	0.000023	0.710098	10	7,733	9.9	−1.72	n.d.	n.d.
C5704 B-9Z-3-1, 23.0–28.0 cm	13.67	Listvenite	0.709741	0.000022	0.709728	61	17,156	8.01	−1.12	n.d.	n.d.
C5704 B-12Z-1, 84.0–89.0 cm	18.72	Listvenite	0.710586	0.000023	0.710546	64	5,844	9.32	−1.98	n.d.	n.d.
C5704 B-14Z-2-1, 25.0–30.0 cm	24.86	Listvenite	0.711991	0.000023	0.711903	144	6,042	10.16	−0.79	0.04	−14.58
C5704 B-14Z-3-1, 71.0–76.0 cm	25.93	Listvenite	0.710479	0.000019	0.710396	143	6,351	10.08	−1.42	1.48	−2.88
C5704 B-16Z-3, 7.0–12.0 cm	28.90	Listvenite	0.710706	0.000021	0.710671	368	38,660	9.42	−1.88	n.d.	n.d.
C5704 B-18Z-3-1, 25.0–31.0 cm	35.34	Listvenite	0.709572	0.000023	0.709430	319	8,284	8.42	0.44	1.49	n.d.
C5704 B-20Z-1, 78.0–83.0 cm	40.01	Listvenite	0.711351	0.000022	0.711339	152	48,281	8.46	0.18	n.d.	n.d.
C5704 B-23Z-1-1, 37.0–42.0 cm	48.75	Listvenite	0.711299	0.000019	0.711297	80	142,571	10.63	−0.82	0.07	−19.07
C5704 B-25Z-2-1, 55.0–60.0 cm	52.45	Listvenite	0.711671	0.000020	0.711670	78	186,366	5.78	−0.21	0.02	−17.36
C5704 B-26Z-2-1, 77.0–82.0 cm	56.11	Listvenite	0.712288	0.000019	0.712175	682	22,385	8.76	−0.23	n.d.	n.d.
C5704 B-28Z-1, 69.0–74.0 cm	60.47	Listvenite	0.710697	0.000020	0.710644	272	18,688	8.86	0.02	0.09	−13.68
C5704 B-30Z-2-1, 53.0–58.0 cm	63.07	Listvenite	0.710541	0.000021	0.710526	318	78,656	9.82	−2.31	n.d.	n.d.
C5704 B-31Z-3-1, 31.0–37.0 cm	65.71	Listvenite	0.711957	0.000019	0.711952	159	138,703	10.3	−2.20	0.22	−6.87
C5704 B-32Z-1-1, 19.0–24.0 cm	66.87	Listvenite	0.711964	0.000020	0.711947	386	85,105	8.92	−1.03	0.88	−4.52
C5704 B-32Z-2-1, 7.0–12.0 cm	67.55	Listvenite	0.713559	0.000019	0.713556	115	174,106	10.61	−1.13	2.43	n.d.
C5704 B-35Z-1-1, 6.0–11.0 cm	71.54	Listvenite	0.712255	0.000022	0.712220	98	10,237	7.23	1.11	0.89	n.d.
C5704 B-38Z-3, 86.0–91.0 cm	80.90	Serpentinite	0.710893	0.000022	0.710876	310	66,812	5.33	−2.37	0.09	−10.07
C5704 B-39Z-1-1, 25.0–30.0 cm	82.18	Serpentinite	0.709307	0.000022	0.709289	48	9,733	2.23	−5.35	0.10	−13.67
C5704 B-39Z-3-1, 13.0–18.0 cm	83.81	Serpentinite	0.710489	0.000021	0.710485	19	15,271	1.96	−6.08	0.03	−22.04
C5704 B-40Z-3-1, 3.0–8.0 cm	86.98	Serpentinite	0.710374	0.000019	0.710372	59	211,715	8.81	−4.91	0.06	−24.23
C5704 B-42Z-2-1, 26.0–31.0 cm	91.85	Serpentinite	0.711831	0.000021	0.711829	18	35,313	1.71	−4.40	0.07	n.d.
C5704 B-43Z-2-1, 3.0–8.0 cm	94.96	Serpentinite	0.712288	0.000019	0.712288	6	89,171	1.87	−4.51	0.07	n.d.
C5704 B-44Z-2-1, 29.0–34.0 cm	98.17	Serpentinite	0.712409	0.000019	0.712409	21	110,987	4.52	−3.17	0.04	−15.24
C5704 B-44Z-3-1, 57.0–62.0 cm	99.31	Serpentinite	0.712489	0.000023	0.712487	37	83,218	3.16	−3.08	0.06	−26.45
C5704 B-44Z-4, 50.0–55.0 cm	99.94	Serpentinite	0.712702	0.000020	0.712701	47	221,049	8.11	−3.42	0.29	−4.90
C5704 B-47Z-3-1, 18.0–23.0 cm	107.88	Listvenite	0.713413	0.000020	0.713040	2,612	25,806	9.26	0.10	0.05	−23.97
C5704 B-48Z-3-1, 26.0–31.0 cm	110.52	Listvenite	0.713068	0.000022	0.712813	2,429	35,139	n.d.	n.d.	0.02	−25.40
C5704 B-48Z-3-1, 90.0–95.0 cm	111.50	Listvenite	0.713178	0.000023	0.713176	33	46,533	8.74	0.66	n.d.	n.d.
C5704 B-50Z-4-1, 65.0–70.0 cm	115.53	Listvenite	0.713420	0.000023	0.712562	8,287	35,574	6.55	0.32	n.d.	n.d.
C5704 B-52Z-1-1, 60.0–65.0 cm	119.13	Listvenite	0.713866	0.000019	0.712775	11,406	38,542	8.1	0.49	0.44	−5.64
C5704 B-52Z-3, 0.0–5.0 cm	119.67	Listvenite	0.714587	0.000022	0.712099	13,213	19,572	9.72	−0.44	n.d.	n.d.
C5704 B-52Z-3-1, 61.0–66.0 cm	120.28	Listvenite	0.713418	0.000019	0.710790	14,220	19,930	8.64	0.10	n.d.	n.d.
C5704 B-54Z-2-1, 47.0–52.0 cm	125.92	Listvenite	0.713753	0.000022	0.709909	16,514	15,830	9.15	0.36	n.d.	n.d.
C5704 B-55Z-1-2, 8.0–13.0 cm	127.76	Listvenite	0.713947	0.000022	0.710839	16,596	19,674	8.37	1.20	0.07	n.d.
C5704 B-55Z-2-1, 59.0–64.0 cm	129.16	Listvenite	0.711807	0.000020	0.711489	3,417	39,477	8.84	−0.37	0.11	−4.23
C5704 B-55Z-3-1, 15.0–20.0 cm	129.65	Listvenite	0.711228	0.000022	0.710116	9,522	31,563	7.87	0.16	n.d.	n.d.
C5704 B-56Z-4-1, 11.0–16.0 cm	133.29	Listvenite	0.712467	0.000022	0.711944	11,464	80,713	9.11	1.52	n.d.	n.d.
C5704 B-60Z-1, 12.0–17.0 cm	140.00	Listvenite	0.712340	0.000022	0.709278	9,275	11,158	8.69	0.61	n.d.	n.d.
C5704 B-60Z-3-1, 40.0–45.0 cm	141.79	Listvenite	0.714136	0.000019	0.712178	15,152	28,514	7.22	0.35	0.31	0.74
C5704 B-60Z-4-1, 24.0–29.0 cm H	142.43	Listvenite	0.714493	0.000020	0.711488	16,037	19,667	8.21	0.93	n.d.	n.d.
C5704 B-64Z-4-1, 18.0–23.0 cm	154.95	Listvenite	0.713390	0.000020	0.711421	12,775	23,908	8.68	1.93	n.d.	n.d.

Table 1
Continued

Sample	Depth (m)	Lithology	$^{87}Sr/^{86}Sr$	2SE total error	$^{87}Sr/^{86}Sr$ at 96 Ma	Rb (ppb)[a]	Sr (ppb)[a]	TC (wt%)	TC $\delta^{13}C$ (‰ V-PDB)	OC (wt%)	TOC $\delta^{13}C$ (‰ V-PDB)
C5704 B-65Z-3-1, 33.0–38.0 cm	156.91	Listvenite	0.712289	0.000020	0.711892	1,079	10,005	10.76	1.41	0.10	−16.35
C5704 B-66Z-3, 66.0–71.0 cm	160.62	Listvenite	0.712607	0.000022	0.711443	11,964	37,852	8.31	0.45	0.06	−24.15
C5704 B-67Z-2-1, 26.0–31.0 cm	162.03	Listvenite	0.713829	0.000022	0.713190	3,747	21,596	8.48	0.55	n.d.	n.d.
C5704 B-67Z-4-1, 39.0–44.0 cm	163.67	Listvenite	0.713195	0.000019	0.711422	10,001	20,778	8.89	1.10	0.04	−10.87
C5704 B-69Z-2, 55.0–63.0 cm	168.38	Listvenite	0.711795	0.000023	0.711591	2,341	42,165	8.98	0.13	n.d.	n.d.
C5704 B-71Z-4, 0.0–8.0 cm	175.63	Listvenite	0.712534	0.000018	0.712196	3,745	40,763	7.12	−0.13	0.05	−16.71
C5704 B-73Z-1, 71.0–75.0 cm	180.01	Listvenite	0.712392	0.000022	0.712335	254	16,269	9.1	0.63	0.24	−4.63
C5704 B-73Z-2, 0.0–5.0 cm	180.30	Listvenite	0.712180	0.000020	0.712145	292	30,626	10.04	−1.53	0.21	−8.61
C5704 B-73Z-3, 8.0–13.0 cm	181.10	Listvenite	0.711917	0.000022	0.711896	1,021	182,886	6.79	−1.29	0.02	−14.10
C5704 B-73Z-4, 11.0–16.0 cm	181.85	Serpentinite	0.710548	0.000022	0.710536	182	57,427	1.62	−2.89	0.04	−16.58
C5704 B-74Z-1, 56.0–64.0 cm	182.95	Serpentinite	0.709169	0.000023	0.708977	2,073	39,906	1.45	−4.90	0.05	−27.04
C5704 B-74Z-2, 0.0–5.0 cm	183.07	Serpentinite	0.709779	0.000017	0.709761	61	13,067	1.88	−7.72	0.07	−10.96
C5704 B-74Z-3, 42.0–47.0 cm	184.24	Serpentinite	0.709023	0.000019	0.708973	294	21,788	0.2	−10.62	0.04	−24.59
C5704 B-74Z-3, 67.0–73.0 cm	184.49	Serpentinite	0.710047	0.000023	0.710033	49	13,717	1.77	−5.40	0.24	−9.94
C5704 B-75Z-1, 12.0–16.0 cm	185.52	Listvenite	0.711230	0.000022	0.711220	134	49,603	12.12	−0.43	0.10	−17.53
C5704 B-75Z-1, 70.0–75.0 cm	186.10	Listvenite	0.711760	0.000020	0.711751	247	110,258	9.7	−0.16	0.16	n.d.
C5704 B-75Z-2, 27.0–32.0 cm	186.46	Listvenite	0.711509	0.000022	0.711497	373	111,620	8.61	−1.00	0.07	n.d.
C5704 B-75Z-2, 31.0–40.0 cm	186.54	Listvenite	0.711653	0.000021	0.711641	272	84,029	9.54	−1.32	0.11	−11.87
C5704 B-75Z-2, 76.0–82.0 cm	186.95	Listvenite	0.712328	0.000019	0.712327	76	244,293	10.73	−2.27	0.69	n.d.
C5704 B-76Z-2, 38.0–42.0 cm	189.58	Listvenite	0.712478	0.000019	0.712476	111	227,322	11.43	−1.64	0.33	−12.42
C5704 B-77Z-3, 40.0–48.0 cm	193.71	Listvenite	0.712441	0.000019	0.712406	1,696	178,429	8.98	−2.12	0.26	−5.61
C5704 B-77Z-4, 43.0–48.0 cm	194.57	Listvenite	0.712800	0.000020	0.712779	1,072	192,155	8.66	−0.71	0.17	−9.16
C5704 B-82Z-1, 50.0–55.0 cm	201.18	Greenschist	0.707364	0.000020	0.705870	70,152	173,001	0.02	n.d.	n.d.	n.d.
C5704 B-88Z-2, 76.0–82.0 cm	214.59	Greenschist	0.707171	0.000018	0.705603	77,502	182,069	0.05	n.d.	n.d.	n.d.
C5704 B-90Z-3, 8.0–13.0 cm	220.79	Greenschist	0.706104	0.000019	0.705707	36,796	341,585	0.03	n.d.	n.d.	n.d.
C5704 B-92Z-3-1, 0.0–8.0 cm	223.58	Greenschist	0.706444	0.000020	0.705879	40,839	266,694	0.02	n.d.	n.d.	n.d.
C5704 B-96Z-2-1, 0.0–8.0 cm	232.10	Greenschist	0.706225	0.000019	0.706131	11,143	436,010	n.d.	n.d.	0.09	−19.25
C5704 B-100Z-2-1, 13.0–21.0 cm	244.47	Greenschist	0.706038	0.000018	0.705968	9,065	477,887	0.25	−0.42	n.d.	n.d.
C5704 B-105Z-4, 31.0–36.0 cm	261.44	Greenschist	0.705739	0.000019	0.705667	10,901	558,612	0.04	n.d.	n.d.	n.d.
C5704 B-109Z-4-1, 24.0–32.0 cm	270.50	Greenschist	0.705247	0.000020	0.705133	17,054	553,129	0.11	n.d.	n.d.	n.d.
C5704 B-116Z-1-1, 31.0–39.0 cm	283.35	Greenstone	0.704564	0.000019	0.704497	7,182	392,644	0.04	n.d.	n.d.	n.d.
C5704 B-124Z-1-1, 53.0–61.0 cm	294.32	Greenstone	0.705393	0.000018	0.705315	11,092	527,027	0.07	n.d.	n.d.	n.d.

Note. SE = Standard error, TC = Total Carbon, TOC = Total Organic Carbon, V-PDB = Vienna Pee Dee Belemnite standard, n.d. = not determined.
[a]Data from Godard et al. (2021).

4.1. Strontium Isotopes

Measured $^{87}Sr/^{86}Sr$ values in Oman DP Hole BT1B lithologies show clear differences between (a) the metamorphic sole and (b) the listvenites and serpentinites. The listvenites and serpentinites vary from a minimum value of 0.709 in the upper serpentinite band to a maximum of 0.715 in some listvenites. $^{87}Sr/^{86}Sr$ values in the listvenites increase with depth from the surface to 150 m while the serpentinite band between 80 and 100 m have lower values. Below 150 m, $^{87}Sr/^{86}Sr$ values are relatively constant with increasing depth, until the second serpentine band at 181–186 m. Below the basal thrust, $^{87}Sr/^{86}Sr$ values are significantly lower in the metamorphic sole from 0.704 to 0.706, followed by lower $^{87}Sr/^{86}Sr$ values with greater depths (Figure 2). Although the metamorphic sole contains meta-basalts (Godard et al., 2021; Kelemen et al., 2021; Kotowski et al., 2021; Searle & Malpas, 1980),

Table 2
Lithological Information, Location, Strontium, Rubidium, and Carbon Concentrations and Sr and C Isotope Data of Samples for Hawasina and Metamorphic Sole Samples

Sample	Latitute	Longitude	Elevation (m)	Distance from basal thrust (m)	Formation	Sr (ppm)	Rb (ppm)	$^{87}Sr/^{86}Sr$	2SE total error	$^{87}Sr/^{86}Sr$ at 96Ma	TC (wt%)	$\delta^{13}C$ (‰ V-PDB)
OM20-01	23.3727	58.18973	556	n.a.	Sole metasediments	360.92	3.6	0.709303	0.000008	0.709267	0.99	−0.61
OM20-03	23.35872	58.23122	364	420	Hawasina	19.47	6.38	0.711651	0.000010	0.710444	0.26	−2.79
OM20-05	23.37326	58.21663	468	470	Hawasina	25.23	5.8	0.709051	0.000007	0.708204	0.36	−1.64
OM20-06	23.3763	58.21493	493	640	Hawasina	314.26	44.7	0.713421	0.000007	0.712897	0.04	n.d.
OM20-07	23.37628	58.21508	488	640	Hawasina	382.46	103.96	0.714331	0.000007	0.713329	0.05	n.d.
OM20-08	23.35756	58.21843	418	120	Hawasina	20.15	10.2	0.712658	0.000007	0.710793	0.09	−1.8
OM20-09	23.35744	58.21829	432	100	Hawasina	32.54	56.28	0.717631	0.000006	0.711258	0.04	n.d.
OM20-11	23.35789	58.21856	454	140	Hawasina	16.06	41.9	0.717592	0.000010	0.707980	0.11	−5.52
OM20-12	23.38609	58.14561	262	780	Hawasina	213.39	4.94	0.709668	0.000009	0.709583	9.18	1.36
OM20-13	23.39792	58.18225	278	150	Hawasina	74.29	8.52	0.710519	0.000006	0.710097	1.69	0.59
OM20-14	23.40735	58.15496	269	700	Hawasina	9.9	17.3	0.715785	0.000008	0.709346	0.19	−3.19
OM20-15	23.40758	58.1547	265	700	Hawasina	89.69	5.73	0.709060	0.000009	0.708824	4.93	1.3
OM20-16	23.39377	58.17862	302	560	Sole metasediments	34.61	27.25	0.714708	0.000006	0.711807	0.05	n.d.
OM20-17	23.40754	58.1546	273	700	Hawasina	30.13	121.1	0.724132	0.000009	0.709324	0.06	n.d.
OM20-10	23.35786	58.21854	458	140	Hawasina	27.97	29.92	0.712403	0.000007	0.708462	0.7	−3.64
OM20-18	23.40763	58.15468	275	700	Hawasina	484.97	4.07	0.708264	0.000009	0.708233	11.06	1.26
OM20-19	23.39655	58.04998	310	300	Hawasina	197.35	15.03	0.709083	0.000007	0.708802	1.28	0.93
OM20-42	23.414996	58.161405	253	1,200	Hawasina	138.71	0.32	0.708511	0.000010	0.708503	11.53	3.69
OM20-04a	23.36214	58.23478	384	970	Hawasina	19.13	6.84	0.710833	0.000009	0.709516	0.7	−0.33
OM20-04B	23.36214	58.23478	384	970	Hawasina	10.01	9.86	0.713150	0.000008	0.709521	0.15	−3.5

Note. SE = Standard error, TC = Total Carbon, T V-PDB = Vienna Pee Dee Belemnite standard, n.a. = not available, n.d. = not determined.

all of the samples have higher $^{87}Sr/^{86}Sr$ than typical mid-ocean ridge basalts (MORB) (Gale et al., 2013; Hofmann, 2013). The Sr isotope values of the listvenite and serpentinite samples from BT1B are similar to those of listvenites in nearby outcrops (Falk & Kelemen, 2015, Figure 2), which are significantly more radiogenic than $^{87}Sr/^{86}Sr$ values of Oman peridotites (Gerbert-Gaillard, 2002; Lanphere et al., 1981; McCulloch et al., 1981) and Cretaceous to modern seawater (McArthur et al., 2001), but less radiogenic than some Hawasina and autochthonous sediments (Weyhenmeyer, 2000). Our serpentinites and listvenites are enriched in Sr and more radiogenic than similar litologhies in the Birjand ophiolite in eastern Iran (Boskabadi et al., 2020). Our samples of the Hawasina metasediments, and those collected from the same region by Falk and Kelemen (2015) have $^{87}Sr/^{86}Sr$ values ranging from 0.7082 to 0.7241. Six of these Hawasina samples are more radiogenic than any of the samples from Hole BT1B (Figure 3).

4.2. Carbon Concentrations and $\delta^{13}C$

4.2.1. Total Carbon

The carbon contents of samples from Hole BT1B are highly dependent on lithology (Figure 2). All samples of ultramafic origin contain some carbon, mainly as Mg-rich carbonates, with serpentinites containing 0.2–5 wt% carbon, and listvenites containing 6–12 wt%. Samples from the metamorphic sole below 200 m depth contain 0.02–0.27 wt% carbon. In contrast, the Hawasina metasediments have highly variable carbon contents. Some are almost pure metamorphosed limestones and dolomites with carbon contents of up to 11 wt%, while some have less than 0.05 wt% carbon.

$\delta^{13}C$ in the upper 200m of Hole BT1B varies significantly between serpentinites and listvenites (Figure 2). Serpentinites contain significantly lighter carbon than listvenites, as observed in the depth profile (Figure 2). The

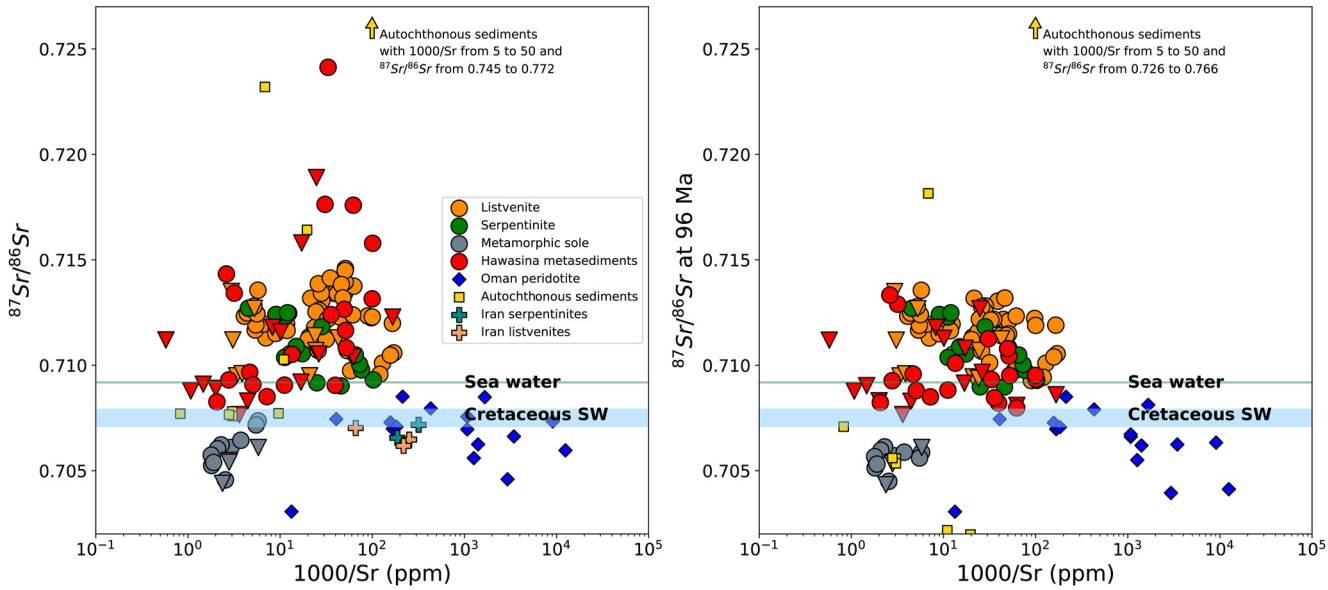

Figure 3. $^{87}Sr/^{86}Sr$ values, both measured (left) and age corrected to 96 Ma (right), plotted versus inverse Sr concentration for core samples from OmanDP Hole BT1B and other lithologies measured in Oman and Iran. Data from Falk and Kelemen (2015) for samples of the same lithologies as those documented here are shown as inverted triangles, employing the same color scheme as used for samples in this study. Data for Hawasina sediments are from this study and Falk and Kelemen (2015), those for Oman peridotites are from Gerbert-Gaillard (2002, leached samples only), those for autochthonous sediment samples are from Weyhenmeyer (2000), and those for Iran samples are from Boskabadi et al. (2020). Rb concentrations were not reported for the autochthonous clastic metasediments from Weyhenmeyer (2000), so we assume an Rb upper bound concentration of 200 ppm (twice the maximum measured in Hawasina metasediments). This Rb concentration was used with the measured $^{87}Sr/^{86}Sr$ and Sr concentration, to estimate a minimum Sr isotope ratio at 96 Ma for these samples. Seawater and Cretaceous seawater values from McArthur et al. (2001).

lower serpentinite band contains two samples (74-2 0.0–5.0 cm and 74-3 42.0–47.0 cm) that contain significantly lighter carbon than any serpentinite in the upper band. In general, carbon concentrations correlate positively with $\delta^{13}C$ values in the upper 200 m (Figure 4). Metamorphic sole samples in the bottom 100 m have low carbon contents and did not yield enough CO_2 for isotopic analysis. Total carbon $\delta^{13}C$ values in the Hawasina nappes range from −5.52‰ to 3.69‰, which almost encompasses the entire range of variation observed in Hole BT1B and appears to decrease with lower carbon contents.

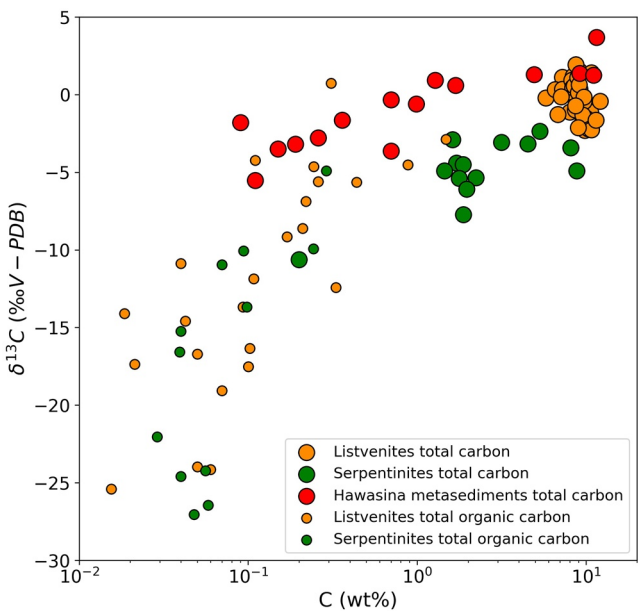

Figure 4. Total Carbon (large circles) and Total Organic Carbon (small circles) versus $\delta^{13}C$ for listvenites, serpentinites, and Hawasina metasediments.

4.2.2. Organic Carbon

Graphitic carbon was identified in the core both at the drill site and during core inspection aboard the D/V Chikyu (Kelemen et al., 2020a; Kelemen et al., 2020b; Kelemen et al., 2021). This organic component has a characteristic low $\delta^{13}C$ signature in listvenites and serpentinites from Hole BT1B, which extends to a minimum of −27.04‰, representing 0.05wt% of total carbon in the sample from 74-1 56.0–64.0 cm (Figure 4). In some cases, the intermediate values likely represent mixtures of organic and inorganic carbon, as some of the magnesite in the listvenites is very resistant to 3N HCl attack and remain undissolved even after 5 days of leaching. The observed light isotopic compositions are similar to those observed in other ultramafic localities such as Cerro de Almirez and Liguria (Alt et al., 2013). These data confirm the presence of organic carbon in Hole BT1B, which was observed during drilling operations, core description aboard D/V Chikyu, and via Raman spectroscopy (Kelemen et al., 2020a; Kelemen et al., 2020b; Kelemen et al., 2021).

5. Discussion

5.1. Temperature and Pressure of Listvenite Formation

Falk and Kelemen (2015) estimated the temperature range of listvenite formation based on conventional and clumped stable isotope thermometry (90 ± 15°C), phase equilibria (80–130°C), and rock textures. New clumped isotope measurements on BT1B drill core samples by Beinlich et al. (2020) widened the temperature range of listvenite formation and/or cooling from ~50 ± 5°C to 250 ± 50°C. This range of values suggests that the infiltrating reactive fluids had variable temperatures, and/or clumped isotope values were reset during cooling, as proposed for fine-grained samples of peridotite-hosted carbonate veins (Garcia del Real et al., 2016). The pressure of listvenite formation is very poorly constrained due to the lack of pressure-sensitive assemblages and the small size of fluid inclusions. A minimum pressure of 0.3 GPa is provided by the P-T conditions recorded by the Arabian carbonate platform during ophiolite obduction (Grobe et al., 2019). For the upper limit, the listvenites must have formed at a pressure below the maximum pressure reported for the metamorphic sole (~1.4 GPa) (Cowan et al., 2014; Searle & Cox, 2002).

5.2. Timing of Listvenite Formation

Falk and Kelemen (2015) used Rb/Sr and $^{87}Sr/^{86}Sr$ data on mineral separates to produce an imprecise isochron age of 97 ± 29 Ma for a listvenite sample. This age is broadly consistent with the ~96 Ma age of formation of igneous crust in the ophiolite, along with the same age of metamorphism for the underlying metamorphic sole just beneath the basal thrust of the ophiolite (Hacker, 1994; Hacker et al., 1996; Rioux et al., 2013, 2016). Moreover, listvenites are found in and near the basal thrust, from the UAE near the northwestern end of the ophiolite outcrop to the area around Hole BT1B, near the southeastern end of the ophiolite outcrop in Oman (Nasir et al., 2007; Stanger, 1985). The extensive outcrop NE of Hole BT1B, known informally as MoD Mountain, exposes the Banded Horizon, a peridotite unit found at the base of the ophiolite mantle section composed of alternating 1-m to 10-m scale bands of dunite, harzburgite, and minor lherzolite. This unit has distinct geochemical characteristics, with higher Al and middle rare-earth-elements, compared to the residual mantle harzburgites that comprise most of the mantle section of the ophiolite (Boudier et al., 1988; Godard et al., 2021; Khedr et al., 2014; Prigent et al., 2018; Yoshikawa et al., 2015). The BT1B listvenites have compositions suggesting that they were formed after basal peridotites from the Banded Horizon (Godard et al., 2021).

Throughout this region, the contacts of listvenite bands within and at the base of the Banded Unit are broadly parallel to banding in the peridotite, and to the contacts between listvenite, peridotite, metamorphic sole, and the Hawasina nappe. These data are consistent with our hypothesis that most of the listvenites formed by alteration of mantle peridotite during the subduction of the underlying sediments via intra-oceanic thrusting and/or later emplacement of the ophiolite onto the Arabian continental margin.

On the basis of steep, fault-bounded contacts of listvenite with young, post-emplacement conglomerates, several workers have inferred that the listvenites formed during later uplift and extension (Nasir et al., 2007; Stanger, 1985; Wilde et al., 2002). Recently, Scharf et al. (2020) reported 60 ± 16 Ma and 58 ± 6 Ma U/Pb ages for two carbonate veins that cut listvenite, and structural observations indicating a top-down sense of shear along some faulted listvenite-peridotite and listvenite-sole contacts. Following prior interpretations, they interpret these ages as formation ages of the listvenites after ophiolite emplacement during uplift of the nearby Jebel Akdar and Saih Hatat anticlinoria. We find that their interpretation is inconsistent with the field observations reported above and evidence of a multistage tectonic overprint after peridotite carbonation and listvenite formation as reported by Menzel et al. (2020) and Kelemen et al. (2020a) and Kelemen et al. (2020b).

We have age-corrected our $^{87}Sr/^{86}Sr$ to the 96 Ma age reported by Falk and Kelemen (2015). This correction gives the lowest possible $^{87}Sr/^{86}Sr$ for all the samples based on reported ages. For the corrections, we used Sr and Rb concentrations reported by Godard et al. (2021) for Hole BT1B and our analyses of Hawasina metasediments. While Rb/Sr is low in most BT1B samples and thus age corrections are small, this correction removes some of the apparent trends observed in measured $^{87}Sr/^{86}Sr$ versus depth. The age corrections particularly affect listvenites with relatively abundant chromian mica (fuchsite-muscovite solid solutions, Falk & Kelemen, 2015, Supporting Information) in the 115–163 m depth interval, as these micas host abundant Rb (Godard et al., 2021). The age correction also affects the estimated $^{87}Sr/^{86}Sr$ values of the metamorphic sole of BT1B and some of the

Hawasina metasediments as their Sr and Rb concentrations are heterogeneous, ranging from 9 to 638 ppm for Sr and 0.4–97.7 ppm for Rb. Regardless, the age-corrected $^{87}Sr/^{86}Sr$ values of the listvenites are much higher than those of the mantle and Cretaceous seawater.

5.3. Fluid Source for Carbonation of Peridotites in Oman DP Hole BT1B

$^{87}Sr/^{86}Sr$ and $d^{13}C$ data on MoD Mountain listvenites and Hole BT1B samples suggest that replacement of peridotite by serpentinite and listvenite resulted from reaction with a single fluid along a reaction path (Kelemen et al., 2021). The initial fluid was far from equilibrium with peridotite, which converted olivine and serpentine in the protolith to carbonates + quartz and approached equilibrium with serpentinite at higher extents of reaction progress and lower integrated water/rock ratios (Beinlich et al., 2020; Kelemen et al., 2021). Mg isotope data from a set of samples studied by Falk and Kelemen (2015) show significant differences between dolomite and magnesite listvenites. Dolomite listvenites (average $\delta^{26}Mg \sim -1.33‰$) are lighter in Mg isotopes than magnesite listvenites (average $\delta^{26}Mg \sim -0.33‰$) (de Obeso et al., 2021), which suggests magnesite dissolution and dolomite formation. This is consistent with the modeled evolution of listvenites during fluid-rock reaction, with dolomite replacing magnesite at increasing water/rock ratios (Kelemen et al., 2021). The process of formation of dolomite veins at the expense of magnesite has been documented in other Cretaceous ophiolites (Boskabadi et al., 2020).

As noted above, after the magnesite and dolomite listvenites formed they were cataclastically deformed, and then cut by late Ca-rich carbonate veins (Menzel et al., 2020). Thus, one might expect the veins to have formed from a later, geochemically distinctive fluid as suggested by variable clumped isotope ($\Delta 47$) derived temperatures (Beinlich et al., 2020) and changes in geochemical signatures in dolomite-dominated intervals (Godard et al., 2021). This can be further addressed in future studies via careful sampling of the post-cataclastic veins and dolomite-rich domains.

Returning attention to the source of the fluid that formed the bulk of the listvenites, assuming that Sr and CO_2 were derived from the same fluid, Sr isotopes can be used to constrain the source of the carbonating fluids that formed the serpentinites and listvenites. Falk and Kelemen (2015) proposed three possible sources of fluids for carbonation: (a) compaction of pore waters from underlying Hawasina metasediments, (b) low-temperature dehydration of opal and clay minerals in calcite-bearing Hawasina metasediments, and (c) higher-grade metamorphic devolatilization reactions involving subducted sediments similar to the Hawasina metasediments coupled with fluid that migrated up the subduction zone.

Unlike younger, mantle-peridotite-hosted carbonates, the listvenites do not contain a significant fraction of seawater- or groundwater-derived Sr (de Obeso & Kelemen, 2018; Gerbert-Gaillard, 2002; Kelemen et al., 2011; Weyhenmeyer, 2000). The listvenites have $^{87}Sr/^{86}Sr$ ratios that are distinct from recent, low-temperature carbonate veins and travertine in the mantle section of the ophiolite (de Obeso & Kelemen, 2018; Kelemen et al., 2011; Weyhenmeyer, 2000). Almost all of the listvenites and associated serpentinites from BT1B core and MoD Mountain outcrops have $^{87}Sr/^{86}Sr$ ratios at 96 Ma higher than Cretaceous seawater (Falk & Kelemen, 2015, and this study). In contrast, young, peridotite-hosted carbonate veins and travertines in the Samail ophiolite consistently have $^{87}Sr/^{86}Sr$ lower than 0.709 and appear to contain mixtures of Sr derived from seawater or groundwater and the mantle (de Obeso & Kelemen, 2018; Gerbert-Gaillard, 2002; Kelemen et al., 2011; Weyhenmeyer, 2000).

Core samples of the sole have $^{87}Sr/^{86}Sr$ ratios that are similar to Indian Ocean MORB and near-ridge Pacific seamounts (Hofmann, 2013), which are systematically lower than the Sr isotope ratios of the listvenites. Perhaps the metamorphic sole metabasalts are remnants of a subducted seamount, similar to accreted seamounts along the Cascadia margin of North America (e.g., Duncan, 1982), which derived from the enriched mantle source of some Indian Ocean MORB. Alternatively, the $^{87}Sr/^{86}Sr$ ratios may have increased during alteration. The stark difference in $^{87}Sr/^{86}Sr$ between the metamorphic sole and the listvenites indicates that fluids derived from the sole are not responsible of the $^{87}Sr/^{86}Sr$ enrichment observed in the ultramafic lithologies in Wadi Mansah.

In contrast, age-corrected Sr isotope ratios for Hawasina metasediments underlying the ophiolite and the metamorphic sole, north and northeast of Hole BT1B, have $^{87}Sr/^{86}Sr$ up to 0.7134 at 96 Ma (Figure 2). The samples with the most radiogenic $^{87}Sr/^{86}Sr$ are clastic sediments containing minor amounts of carbonates. Hawasina limestones, on the other hand, have lower $^{87}Sr/^{86}Sr$ values, which is consistent with calcite precipitated from seawater that incorporated a minor, radiogenic clastic component. Based on these observations, the most likely source of the fluids that formed the listvenites are derived from the Hawasina metasediments.

Thermodynamic modeling of fluid-rock reactions (Kelemen et al., 2021) shows that the characteristic listvenite mineral assemblages—magnesite + quartz—are attained from fluids with ~20,000 ppm dissolved C for listvenite formation at 100–300°C and 0.5–1 GPa, similar to the assemblages modeled by Klein and Garrido (2011) at lower pressures. Such high dissolved carbon contents are impossible to attain by congruent dissolution of pure calcite in aqueous fluids at these P-T conditions (Kelemen & Manning, 2015), which rules out silicate-poor limestones such as those from the continental margin as a carbon source. On the other hand, metamorphic devolatilization of rocks composed of silicate-carbonate mixtures can produce C-rich fluids at temperatures above 400°C and low to moderate pressures, depending on the rock composition. Thus, we infer that the fluids that formed the listvenites derived from devolatilization of subducting metasediments. During prograde subduction metamorphism, calc-silicate rocks, containing both clastic and carbonate components, undergo extensive devolatilization at 2–3 GPa and 500–700°C (Gorman et al., 2006; Stewart & Ague, 2020) and lose significant amounts of their CO_2 in this PT range due to reactions similar to the simplified reaction:

$$CaMg(CO_3)_2\,(\text{dolomite}) + CaMgSi_2O_6\,(\text{diopside}) + 2\ CaAl_2Si_2O_7(OH)_2\cdot H_2O\ (\text{lawsonite})$$

$$= 2\ Ca_2MgAl_2Si_3O_{12}\,(\text{garnet}) + 4\ H_2O + 2\ CO_2$$

In contrast, carbonate-rich compositions (limestone, dolomite, marble) are predicted to retain most of their CO_2 during subduction (e.g., Kerrick & Connolly, 2001; Stewart & Ague, 2020).

These decarbonation reactions are possible for both the metamorphic sole and Hawasina sediments. The modeling approach of Kelemen et al. (2021) suggests that fluids derived from the sole and clastic Hawasina metasediments will have enough dissolved carbon to react with peridotite and result in magnesite-quartz rocks, the characteristic listvenite assamblage. However, if fluids derived from the sole are the source of the carbon, admixing of a different fluid derived from Hawasina metasediments is required to explain the $^{87}Sr/^{86}Sr$ measured in the listvenites. On the other hand, Kelemen et al. show that fluids derived from a rock with composition analogous to Hawasina OM20-17 contain enough dissolved carbon for serpentinization and carbonation of peridotite with increasing water/rock (W/R) ratios. This, combined with the radiogenic $^{87}Sr/^{86}Sr$ composition of OM20-17, suggests that a single fluid could be responsible for carbonation of the peridotites. We test this scenario using the reaction path proposed by Kelemen et al. (2021). Their model generates a fluid with ~14,000 ppm carbon at 400°C and 1 GPa from decarbonation of a rock with composition such as OM20-17. Under these modeled conditions (400°C, 1 GPa), a lithology like OM20-17 will lose ~65% of its carbon, other Hawasina samples require less decarbonation to produce fluids capable of carbonating the peridotites. If this fluid is then cooled to 200°C and depressurized to 0.5 GPa without losing much of its carbon before reacting with peridotites, listvenites are predicted to form at water/rock (W/R)~100.

At temperatures greater than ~300°C, dissolved CO_2 in aqueous fluids have $\delta^{13}C$ values that are higher than those of co-existing calcite and dolomite (Chacko et al., 1991; Deines, 2004; Horita, 2014). Thus, for example, fluid in equilibrium with calcite with $\delta^{13}C$ between −5.5‰ and −3.5‰ (as in Hawasina clastic metasediments) would contain dissolved CO_2 with $\delta^{13}C$ of −1.9‰ to 0.1‰ at 400°C. At lower temperatures, like those estimated for listvenite formation in the Samail ophiolite, calcite and dolomite have $\delta^{13}C$ higher than co-existing fluids. Thus, dolomite and magnesite in equilibrium with fluids with $\delta^{13}C$ of −1.9‰ to 0.1‰ would have $\delta^{13}C$ in the range of −0.2‰ to 1.8‰, similar to the $\delta^{13}C$ observed in the listvenites from Hole BT1B and the surrounding outcrops.

Figure 5a illustrates that the listvenites and serpentinites from Hole BT1B lie along the reaction path used by Kelemen et al. (2021). In our calculations, we assume that reacting fluids enriched in Sr (250 ppm), with $^{87}Sr/^{86}Sr$ values at 96 Ma that are similar to those of clastic Hawasina metasediments (0.7110–0.7135), reacted with the peridotite with mantle-like $^{87}Sr/^{86}Sr$ (0.7027 ± 0.0011). In the model, serpentinites plot at low W/R between 1 and 5 while listvenites require significantly more fluid at W/R between 5 and 100. The listvenites and serpentinites follow a mixing trend (Figure 5b) between mantle peridotite like compositions (Sr = 1.5 ppm, $^{87}Sr/^{86}Sr$ = 0.7027 ± 0.0011, C = 680 ppm and $\delta^{13}C$ = −6.0 ± 2.0‰) and low-temperature carbonates that crystallized from a fluid produced by high-pressure, high-temperature devolatilization with Sr isotope ratios in the range of the Hawasina clastic metasediments (Sr = 250 ppm, $^{87}Sr/^{86}Sr$ ~0.7100–0.7135) and fractionate carbon isotopes as described above. These trends together suggest that the CO_2-bearing aqueous fluids that formed the listvenites from Hole BT1B and surrounding outcrops were derived by devolatilization of calc-silicate

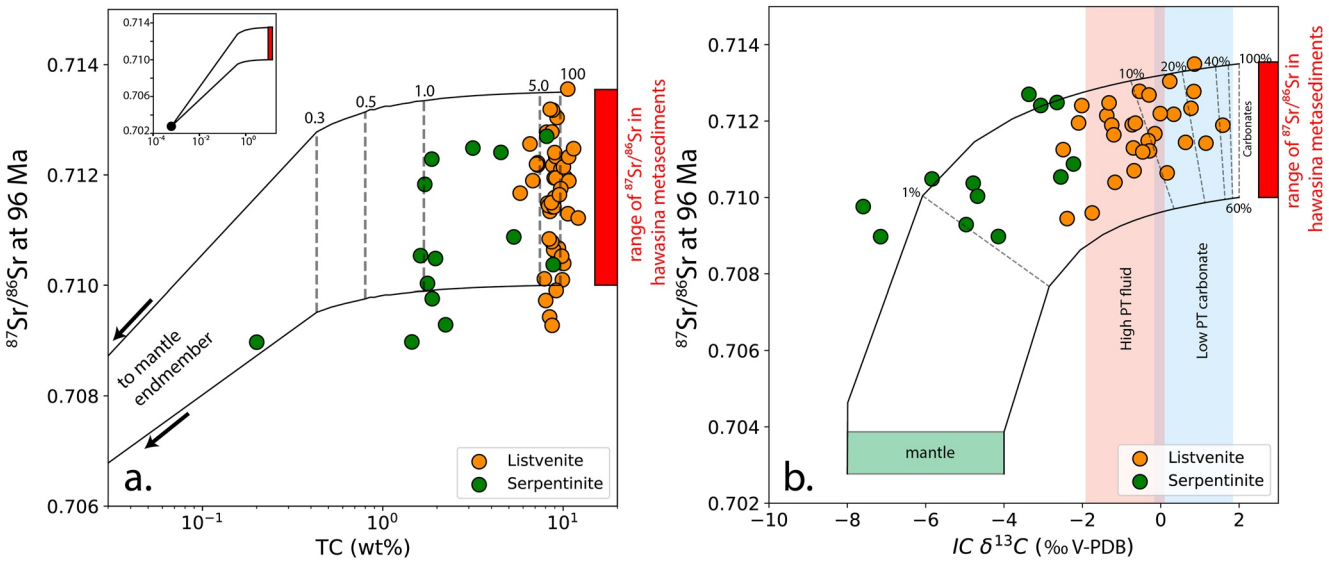

Figure 5. (left) Total carbon (wt%) versus $^{87}Sr/^{86}Sr$ at 96 Ma. Black lines are reaction paths of carbon-rich fluid reacting with peridotite at 200°C and 0.5 GPa at variable water/rock (dashed tie lines) from Kelemen et al. (2021). The reacting fluid is assumed to have $^{87}Sr/^{86}Sr$ values of 0.7100–0.7135 like those of clastic Hawasina metasediments. (right) Inorganic carbon $\delta^{13}C$ versus $^{87}Sr/^{86}Sr$ at 96 Ma. Black lines are mixing lines between mantle and carbonate minerals precipitated from a metamorphic fluid. The fluid has the same carbon concentration as the reaction path in Figure 5a and the $\delta^{13}C$ fractionation between the carbonate and the fluid is described in the body of the text, with values for high and low PT shown as red and blue boxes, respectively. We assume that the fluid has the Sr isotope ratios of Hawasina clastic metasediments. $^{87}Sr/^{86}Sr$ values for the depleted mantle are from mid-ocean-ridge-basalt (MORB) from Hofmann (2013). Mantle $\delta^{13}C$ is from Deines (2002).

metasediments, with $^{87}Sr/^{86}Sr$ and $\delta^{13}C$ similar to clastic sediments in the Hawasina Formation along a subduction zone geotherm. These fluids migrated updip to lower pressures and temperatures to form the listvenites.

6. Conclusions

Listvenites and spatially associated serpentinites from Hole BT1B and surrounding outcrops that replace residual mantle peridotites from the base of the Samail ophiolite have Sr isotope ratios that are more radiogenic than their peridotite protoliths, Cretaceous seawater, modern seawater, groundwater in the ophiolite, and the underlying metamorphic sole. We suggest that the radiogenic Sr isotope component was transported via carbon-rich aqueous fluid that reacted with the peridotite to form the listvenites and serpentinites. The $^{87}Sr/^{86}Sr$ values of this component resemble those of calcite-bearing clastic sediments in the Hawasina Formation underlying the ophiolite. However, the fluid must have contained higher dissolved carbon contents than feasible for congruent dissolution of pure calcite at <2GPa and/or <550°C. Thus, we hypothesize that this fluid was derived by devolatilization of carbonate-bearing and silicate-bearing meta-sediments akin to the Hawasina clastic metasediments at 0.5–2.3 GPa and 400–700°C in the subduction zone (Searle et al., 1994). This fluid then migrated updip to react with hanging wall peridotite at <1 GPa and <250°C, forming the listvenites and serpentinites. Carbon isotope fractionation during high-temperature devolatilization followed by low-temperature carbonate precipitation during the reaction with peridotite likely controlled the isotopic characteristics of the listvenites and the serpentinites with $\delta^{13}C$ from −10.6‰ to 1.92‰ and $^{87}Sr/^{86}Sr$ from 0.7090 to 0.7145.

Appendix A

Oman Drilling Project Phase 1 Science Party

Jürg Matter, University of Southampton, United Kingdom; Damon Teagle, University of Southampton, United Kingdom; Jude Coggon, University of Southampton, United Kingdom; Michelle Harris, Plymouth University, United Kingdom; Emma Bennett, Cardiff University, United Kingdom; Nico Bompard, University of Southampton, United Kingdom; Marine Boulanger, Centre de Recherches Pétrographiques et Géochimiques, France; Lyderic France, Université de Lorraine, France; Gretchen Früh-Green, ETH Zurich, Switzerland; Dieter

Garbe-Schönberg, Christian-Albrecht University of Kiel, Germany; Benoit Ildefonse, Université de Montpellier, France; Ana Jesus, German University of Technology in Oman, Oman; Jürgen Koepke, Leibniz University Hannover, Germany; Louise Koornneef, Plymouth University, United Kingdom; Romain Lafay, University of Lausanne, Switzerland; Johan Lissenberg, Cardiff University, United Kingdom; Chris MacLeod, Cardiff University, United Kingdom; Dominik Mock, Leibniz University of Hanover, Germany; Tony Morris, Plymouth University, United Kingdom; Samuel Müller, Kiel University, Germany; Julie Noël, Université de Montpellier, France; Daniel Nothaft, University of Colorado, USA; Americus Perez, Kanazawa University, Japan; Philippe Pezard, Université de Montpellier, France; Nehal Warsi, AZD Engineering, Oman; David Zeko , University of British Columbia, Canada; Barbara Zihlmann , University of Southampton, United Kingdom; Mohamed-Amine Bechkit , Houari Boumedienne University, Algeria; Laurent Brun, University of Montpellier, France; Bernard Célérier, University of Montpellier, France; Gilles Henry, University of Montpellier, France; Jehanne Paris, University of Montpellier, France; Gérard Lods, University of Montpellier, France; Pascal Robert, Université de Lorraine, Nancy, France; Salim Al Amri, Ministry of Regional Municipalities and Water Resources, Sultanate of Oman; Mohsin Al Shukaili , Ministry of Regional Municipalities and Water Resource, Sultanate of Oman; Ali Al Qassabi , Ministry of Regional Municipalities and Water Resources, Sultanate of Oman; Kyaw Moe, Japan Agency for Marine-Earth Science and Technology (JAMSTEC), Japan; Yasu Yamada, Japan Agency for Marine-Earth Science and Technology (JAMSTEC), Japan; Eiichi Takazawa, Niigata University, Japan; Katsuyoshi Michibayashi, Shizuoka University, Japan; Natsue Abe, JAMSTEC, Japan; Tetsu Akitou , Okayama University, Japan; Salim Ahmed AlShahri, Public Authority for Mining, Oman; Hamood Hamed Shames Al-Siyabi , MRMWR, Oman; Saif Masoud Alhumaimi , Public Authority for Mining, Oman; Maqbool Hussein AlRawahi, MRMWR, Oman; Musaab Shaker Al Sarmi, Sultan Qaboos; University, Oman; Bader Hamed Alwaeli, Sultan Qaboos; University, Oman; Andreas Beinlich, University of Bergen, Norway; Elliot Carter, University of Manchester, United Kingdom; Mike Cheadle, University of Wyoming, USA; Mark Cloos, University of Texas at Austin, USA; Matthew Cooper, University of Southampton, United Kingdom; Laura Crispini, University of Genova, Italy; Joëlle D'Andres (was Ducommun), Australian National University, Australia; Luke Deamer, Cardiff University, United Kingdom; Jeremy Deans, University of Southern Mississippi, USA; Kathi Faak, Ruhr-Universitaet Bochum, Germany; Rebecca Greenberger, California Institute of Technology, USA; Yumiko Harigane, National Institute of Advanced Industrial Science and Technology, Japan; Kohei Hatakeyama, Hiroshima University, Japan; Andrew Horst, Marshall University, USA; Takashi Hoshide, Akita University, Japan; Keisuke Ishii, Niigata University, Japan; Kevin Johnson, University of Hawaii, USA; Michael Kettermann, Aachen University, Germany; Hogyum Kim, Seoul National University, Republic of Korea; Kentaro Kondo, Akita University, Japan; Alissa Kotowski, University of Texas at Austin, USA; Fatna Kourim , Academia Sinica, Taiwan; Yuki Kusano, Geological Survey of Japan, Japan; Catriona Menzies, University of Southampton, United Kingdom; Tomoaki Morishita, Kanazawa University, Japan; Du Khac Nguyen, Kanazawa University, Japan; Toshio Nozaka, Okayama University, Japan; Keishi Okazaki, JAMSTEC, Japan; Suzanne Picazo, University of Lausanne, Switzerland; Ryoko Senda, Kyushu University, Japan; Yamato Tateishi, Okayama University, Japan; Jessica Till, University of Iceland, Iceland; Susumu Umino, Kanazawa University, Japan; Janos Urai, Aachen University, Germany; Yoichi Usui, JAMSTEC, Japan

Acknowledgments

JCO wants to thank Steven Goldstein for allowing early access to the laboratories in LDEO to complete isotope work soon after partial reopening following the first wave of the COVID-19 pandemic in New York. Wei Huang is thanked for help with measurements of carbon concentrations and $\delta^{13}C$. The authors thank Mark Dekkers for editorial handling. Constructive comments from an anonymous Associate Editor, Arman Boskabadi, and an anonymous reviewer helped to improve earlier versions of this manuscript. This research used samples and/or data provided by the Oman Drilling Project. The Oman Drilling Project (OmanDP) has been possible through co-mingled funds from the International Continental Scientific Drilling Project (ICDP; Kelemen, Matter, Teagle Lead PIs), the Sloan Foundation–Deep Carbon Observatory (Grant 2014-3-01, Kelemen PI), the National Science Foundation (NSF-EAR-1516300, Kelemen lead PI), NASA–Astrobiology Institute (NNA15BB02 A, Templeton PI), the German Research Foundation (DFG: KO 1723/21-1, Koepke PI), the Japanese Society for the Promotion of Science (JSPS no:16H06347, Michibayashi PI; and KAKENHI 16H02742, Takazawa PI), the European Research Council (Adv: no.669972; Jamveit PI), the Swiss National Science Foundation (SNF:20FI21_163073, Früh-Green PI), JAMSTEC, the TAMU-JR Science Operator, and contributions from the Sultanate of Oman Ministry of Regional Municipalities and Water Resources, the Oman Public Authority of Mining, Sultan Qaboos University, CNRS-Univ. Montpellier, Columbia University of New York, and the University of Southampton. This research was undertaken thanks in part to funding from the Canada First Research Excellence Fund for JCO.

Data Availability Statement

All data are in the process of being approved by Pangea repository: https://issues.pangaea.de/browse/PDI-30281 and https://issues.pangaea.de/browse/PDI-30282.

References

Alt, J. C., Schwarzenbach, E. M., Früh-Green, G. L., Shanks, W. C., Bernasconi, S. M., Garrido, C. J., et al. (2013). The role of serpentinites in cycling of carbon and sulfur: Seafloor serpentinization and subduction metamorphism. *Lithos*, *178*, 40–54. https://doi.org/10.1016/j.lithos.2012.12.006

Bach, W., Rosner, M., Jöns, N., Rausch, S., Robinson, L. F., Paulick, H., & Erzinger, J. (2011). Carbonate veins trace seawater circulation during exhumation and uplift of mantle rock: Results from ODP Leg 209. *Earth and Planetary Science Letters*, *311*(3–4), 242–252. https://doi.org/10.1016/j.epsl.2011.09.021

Bechennec, F., Le Metour, J., Rabu, D., Bourdillon-de-Grissac, C., de Wever, P., Beurrier, M., & Villey, M. (1990). The Hawasina Nappes: Stratigraphy, palaeogeography and structural evolution of a fragment of the south-Tethyan passive continental margin. *Geological Society Special Publication*, *49*(49), 213–223. https://doi.org/10.1144/GSL.SP.1992.049.01.14

Bechennec, F., Le Métour, J., Rabu, D., Villey, M., & Beurrier, M. (1988). The Hawasina Basin: A fragment of a starved passive continental margin, thrust over the Arabian platform during obduction of the Sumail Nappe. *Tectonophysics*, *151*, 1–343. https://doi.org/10.1016/0040-1951(88)90251-X

Beinlich, A., Plümper, O., Boter, E., Müller, I. A., Kourim, F., Ziegler, M., et al. (2020). Ultramafic rock carbonation: Constraints from listvenite core BT1B, Oman Drilling Project. *Journal of Geophysical Research: Solid Earth*, *125*(6), 1–21. https://doi.org/10.1029/2019jb019060

Beinlich, A., Plümper, O. H., velmann, J., Austrheim, H., & Jamtveit, B. (2012). Massive serpentinite carbonation at Linnajavri, N-Norway. *Terra Nova*, *24*(6), 446–455. https://doi.org/10.1111/j.1365-3121.2012.01083.x

Blakely, R. J., Brocher, T. M., & Wells, R. E. (2005). Subduction-zone magnetic anomalies and implications for hydrated forearc mantle. *Geology*, *33*(6), 445–448. https://doi.org/10.1130/G21447.1

Boskabadi, A., Pitcairn, I. K., Broman, C., Boyce, A., Teagle, D. A. H., Cooper, M. J., et al. (2017). Carbonate alteration of ophiolitic rocks in the Arabian–Nubian Shield of Egypt: Sources and compositions of the carbonating fluid and implications for the formation of Au deposits. *International Geology Review*, *59*(4), 391–419. https://doi.org/10.1080/00206814.2016.1227281

Boskabadi, A., Pitcairn, I. K., Leybourne, M. I., Teagle, D. A. H., Cooper, M. J., Hadizadeh, H., et al. (2020). Carbonation of ophiolitic ultramafic rocks: Listvenite formation in the Late Cretaceous ophiolites of eastern Iran. *Lithos*, *352–353*, 105307. https://doi.org/10.1016/j.lithos.2019.105307

Boudier, F., Ceuleneer, G., & Nicolas, A. (1988). Shear zones, thrusts and related magmatism in the Oman ophiolite: Initiation of thrusting on an oceanic ridge. *Tectonophysics*, *151*(1–4), 275–296. https://doi.org/10.1016/0040-1951(88)90249-1

Braun, M. G. (2004). *Petrologic and Microstructural Constraints on Focused Melt Transport in Dunites and Rheology of the Shallow Mantle*. WHOI/MIT. Retrieved from http://oai.dtic.mil/oai/oai?verb=getRecord&metadataPrefix=html&identifier=ADA426948

Braun, M. G., & Kelemen, P. B. (2002). Dunite distribution in the Oman Ophiolite: Implications for melt flux through porous dunite conduits. *Geochemistry, Geophysics, Geosystems*, *3*(11), 1–21. https://doi.org/10.1029/2001GC000289

Chacko, T., Mayeda, T. K., Clayton, R. N., & Goldsmith, J. R. (1991). Oxygen and carbon isotope fractionations between CO2 and calcite. *Geochimica et Cosmochimica Acta*, *55*(10), 2867–2882. https://doi.org/10.1016/0016-7037(91)90452-B

Clark, I. D., & Fontes, J.-C. (1990). Paleoclimatic reconstruction in northern Oman based on carbonates from hyperalkaline groundwaters. *Quaternary Research*, *33*(3), 320–336. https://doi.org/10.1016/0033-5894(90)90059-T

Collier, M. L. (2012). *Spatial-statistical properties of geochemical variability as constraints on magma transport and evolution processes at ocean ridges*. Columbia University.

Cowan, R. J., Searle, M. P., & Waters, D. J. (2014). Structure of the metamorphic sole to the Oman Ophiolite, Sumeini Window and Wadi Tayyin: Implications for ophiolite obduction processes. *Geological Society Special Publication*, *392*(1), 155–175. https://doi.org/10.1144/SP392.8

Deines, P. (2002). The carbon isotope geochemistry of mantle xenoliths. *Earth-Science Reviews*, *58*(3–4), 247–278. https://doi.org/10.1016/S0012-8252(02)00064-8

Deines, P. (2004). Carbon isotope effects in carbonate systems. *Geochimica et Cosmochimica Acta*, *68*(12), 2659–2679. https://doi.org/10.1016/j.gca.2003.12.002

Delacour, A., Früh-Green, G. L., Bernasconi, S. M., Schaeffer, P., & Kelley, D. S. (2008). Carbon geochemistry of serpentinites in the Lost City Hydrothermal System (30°N, MAR). *Geochimica et Cosmochimica Acta*, *72*(15), 3681–3702. https://doi.org/10.1016/J.GCA.2008.04.039

de Obeso, J. C., & Kelemen, P. B. (2018). Fluid rock interactions on residual mantle peridotites overlain by shallow oceanic limestones: Insights from Wadi Fins, Sultanate of Oman. *Chemical Geology*, *498*, 139–149. https://doi.org/10.1016/J.CHEMGEO.2018.09.022

de Obeso, J. C., & Kelemen, P. B. (2020). Major element mobility during serpentinization, oxidation and weathering of mantle peridotite at low temperatures. *Philosophical Transactions. Series A, Mathematical, Physical, and Engineering Sciences*, *378*(2165), 20180433. https://doi.org/10.1098/rsta.2018.0433

de Obeso, J. C., Ramos, S. D. P., Higgins, J. A., & Kelemen, P. B. (2021). A Mg isotopic perspective on the mobility of magnesium during serpentinization and carbonation of the Oman ophiolite. *Journal of Geophysical Research: Solid Earth*, *126*(2), 1–17. https://doi.org/10.1029/2020JB020237

DeShon, H. R., & Schwartz, S. Y. (2004). Evidence for serpentinization of the forearc mantle wedge along the Nicoya Peninsula, Costa Rica. *Geophysical Research Letters*, *31*(21). https://doi.org/10.1029/2004GL021179

Duncan, R. A. (1982). A captured island chain in the coast range of Oregon and Washington. *Journal of Geophysical Research*, *87*(B13), 10827–10837. https://doi.org/10.1029/JB087iB13p10827

Falk, E. S., & Kelemen, P. B. (2015). Geochemistry and petrology of listvenite in the Samail ophiolite, Sultanate of Oman: Complete carbonation of peridotite during ophiolite emplacement. *Geochimica et Cosmochimica Acta*, *160*, 70–90. https://doi.org/10.1016/j.gca.2015.03.014

Fruh-Green, G. L., Connolly, J. A. D. D., Plas, A., Kelley, D. S., Grobety, B., Früh-Green, G. L., et al. (2004). Serpentinization of oceanic peridotites: Implications for geochemical cycles and biological activity *AGU Monograph*, *144*, 119–136. https://doi.org/10.1029/144GM08

Gale, A., Dalton, C. A., Langmuir, C. H., Su, Y., & Schilling, J. G. (2013). The mean composition of ocean ridge basalts. *Geochemistry, Geophysics, Geosystems*, *14*(3), 489–518. https://doi.org/10.1029/2012GC004334

Garcia del Real, P., Maher, K., Kluge, T., Bird, D. K., Brown, G. E., & John, C. M. (2016). Clumped-isotope thermometry of magnesium carbonates in ultramafic rocks. *Geochimica et Cosmochimica Acta*, *193*, 222–250. https://doi.org/10.1016/j.gca.2016.08.003

Gerbert-Gaillard, L. (2002). Caractérisation Géochimique des Péridotites de l'ophiolite d'Oman : Processus magmatiques aux limites lithosphère/asthenosphère. *Université Montpellier II - Sciences et Techniques du Languedoc*.

Godard, M., Carter, E. J., Decrausaz, T., Lafay, R., Bennett, E., Kourim, F., et al. (2021). Geochemical profiles across the listvenite-metamorphic transition in the basal megathrust of the Semail ophiolite: Results from drilling at Oman DP Hole BT1B. *Journal of Geophysical Research: Solid Earth*, *126*(12), e2021JB022733. https://doi.org/10.1029/2021JB022733

Godard, M., Jousselin, D., & Bodinier, J.-L. (2000). Relationships between geochemistry and structure beneath a palaeo-spreading centre: A study of the mantle section in the Oman ophiolite. *Earth and Planetary Science Letters*, *180*(1–2), 133–148. https://doi.org/10.1016/S0012-821X(00)00149-7

Gorman, P. J., Kerrick, D. M., & Connolly, J. A. D. (2006). Modeling open system metamorphic decarbonation of subducting slabs. *Geochemistry, Geophysics, Geosystems*, *7*(4). https://doi.org/10.1029/2005GC001125

Grobe, A., Von Hagke, C., Littke, R., Dunkl, I., Wübbeler, F., Muchez, P., & Urai, J. L. (2019). Tectono-thermal evolution of Oman's Mesozoic passive continental margin under the obducting Semail Ophiolite: A case study of Jebel Akhdar, Oman. *Solid Earth*, *10*(1), 149–175. https://doi.org/10.5194/se-10-149-2019

Hacker, B. R. (1994). Rapid emplacement of young oceanic lithosphere: Argon geochronology of the Oman ophiolite. *Science*, *265*(5178), 1563–1565. https://doi.org/10.1126/science.265.5178.1563

Hacker, B. R., & Mosenfelder, J. L. (1996). Metamorphism and deformation along the emplacement thrust of the Samail ophiolite. *Oman. Earth and Planetary Science Letters*, *144*(3–4), 435–451. https://doi.org/10.1016/S0012-821X(96)00186-0

Hacker, B. R., Mosenfelder, J. L., & Gnos, E. (1996). Rapid emplacement of the Oman ophiolite: Thermal and geochronologic constraints. *Tectonics*, *15*(6), 1230–1247. https://doi.org/10.1029/96TC01973

Halls, C., & Zhao, R. (1995). Listvenite and related rocks: Perspectives on terminology and mineralogy with reference to an occurrence at Creggan baun, Co. Mayo, Republic of Ireland. *Mineralium Deposita*, *30*(3–4), 303–313. https://doi.org/10.1007/BF00196366

Hanghøj, K., Kelemen, P. B., Hassler, D., & Godard, M. (2010). Composition and genesis of depleted mantle peridotites from the Wadi Tayin Massif, Oman ophiolite; Major and trace element geochemistry, and Os isotope and PGE systematics. *Journal of Petrology*, *51*(1–2), 201–227. https://doi.org/10.1093/petrology/egp077

Hansen, L. D., Dipple, G. M., Gordon, T. M., & Kellett, D. A. (2005). Carbonated serpentinite (listwanite) at Atlin, British Columbia: A geological analogue to carbon dioxide sequestration. *The Canadian Mineralogist*, *43*(1), 225–239. https://doi.org/10.2113/gscanmin.43.1.225

Hofmann, A. W. (2013). Sampling mantle heterogeneity through oceanic basalts: Isotopes and trace elements. *Treatise on geochemistry* (2nd ed., Vol. 3, pp. 67–101). Elsevier Ltd. https://doi.org/10.1016/B978-0-08-095975-7.00203-5

Horita, J. (2014). Oxygen and carbon isotope fractionation in the system dolomite-water-CO2 to elevated temperatures. *Geochimica et Cosmochimica Acta*, *129*, 111–124. https://doi.org/10.1016/j.gca.2013.12.027

Hyndman, R. D., & Peacock, S. M. (2003). Serpentinization of the forearc mantle. *Earth and Planetary Science Letters*, *212*(3–4), 417–432. https://doi.org/10.1016/S0012-821X(03)00263-2

Kamiya, S., & Kobayashi, Y. (2000). Seismological evidence for the existence of serpentinized wedge mantle. *Geophysical Research Letters*, *27*(6), 819–822. https://doi.org/10.1029/1999GL011080

Kelemen, P. B., de Obeso, J. C., Leong, J. A. M., Godard, M., Okazaki, K., Kotowski, A. J., et al. (2021). Mass transfer into the leading edge of the mantle wedge: Initial results from Oman Drilling Project Hole BT1B. *Earth and Space Science Open Archive*, 2021JB022352R. https://doi.org/10.1002/essoar.10507370.1

Kelemen, P. B., & Manning, C. E. (2015). Reevaluating carbon fluxes in subduction zones, what goes down, mostly comes up. *Proceedings of the National Academy of Sciences*, *112*(30), E3997–E4006. https://doi.org/10.1073/pnas.1507889112

Kelemen, P. B., & Matter, J. M. (2008). In situ carbonation of peridotite for CO_2 storage. *Proceedings of the National Academy of Sciences*, *105*(45), 17295–17300. https://doi.org/10.1073/pnas.0805794105

Kelemen, P. B., Matter, J. M., Streit, E. E., Rudge, J. F., Curry, W. B., & Blusztajn, J. (2011). Rates and mechanisms of mineral carbonation in peridotite: Natural processes and recipes for enhanced, in situ CO_2 capture and storage. *Annual Review of Earth and Planetary Sciences*, *39*(1), 545–576. https://doi.org/10.1146/annurev-earth-092010-152509

Kelemen, P. B., Matter, J. M., Teagle, D. A. H., Coggon, J. A., & The Oman Drilling Project Science Team (2020a). Proceedings of the Oman Drilling Project. In *Proceedings of the Oman Drilling Project (Vol. Phase 1 an). International Ocean Discovery Program*. International Ocean Discovery Program. https://doi.org/10.14379/OmanDP.proc.2020

Kelemen, P. B., Matter, J. M., Teagle, D. A. H., Coggon, J. A., & The Oman Drilling Project Science Team (2020b). Site BT1: Fluid and mass exchange on a subduction zone plate boundary. In P. B. Kelemen, J. M. Matter, D. A. H. Teagle, & J. A. Coggond (Eds.), *Proceedings of the Oman Drilling Project*. International Ocean Discovery Program.

Kerrick, D. M., & Connolly, J. A. D. (2001). Metamorphic devolatilization of subducted marine sediments and the transport of volatiles into the Earth's mantle. *Nature*, *411*, 293–296. https://doi.org/10.1038/35077056

Khedr, M. Z., Arai, S., Python, M., & Tamura, A. (2014). Chemical variations of abyssal peridotites in the central Oman ophiolite: Evidence of oceanic mantle heterogeneity. *Gondwana Research*, *25*(3), 1242–1262. https://doi.org/10.1016/J.GR.2013.05.010

Klein, F., & Garrido, C. J. (2011). Thermodynamic constraints on mineral carbonation of serpentinized peridotite. *Lithos*, *126*(3–4), 147–160. https://doi.org/10.1016/j.lithos.2011.07.020

Klein, F., Humphris, S. E., & Bach, W. (2020). Brucite formation and dissolution in oceanic serpentinite. *Geochemical Perspectives Letters*, 1–5. https://doi.org/10.7185/geochemlet.2035

Kotowski, A. J., Cloos, M., Stockli, D. F., & Orent, E. B. (2021). Structural and thermal evolution of an infant subduction shear zone: Insights from sub-ophiolite metamorphic rocks recovered from Oman Drilling Project Site BT-1B. *Journal of Geophysical Research: Solid Earth*, *126*(12), e2021JB021702. https://doi.org/10.1029/2021JB021702

Lanphere, M. A., Coleman, R. G., & Hopson, C. A. (1981). Sr isotopic tracer study of the Samail Ophiolite, Oman. *Journal of Geophysical Research*, *86*(B4), 2709–2720. https://doi.org/10.1029/JB086iB04p02709

Macdonald, A. H., & Fyfe, W. S. (1985). Rate of serpentinization in seafloor environments. *Tectonophysics*, *116*(1–2), 123–135. https://doi.org/10.1016/0040-1951(85)90225-2

McArthur, J. M., Howarth, R. J., & Bailey, T. R. (2001). Strontium isotope stratigraphy: LOWESS version 3: Best fit to the marine Sr-isotope curve for 0–509 Ma and accompanying look-up table for deriving numerical age. *The Journal of Geology*, *109*(2), 155–170. https://doi.org/10.1086/319243

McCulloch, M. T., Gregory, R. T., Wasserburg, G. J., & Taylor, H. P. (1981). Sm-Nd, Rb-Sr, and18O/16O isotopic systematics in an oceanic crustal section: Evidence from the Samail ophiolite. *Journal of Geophysical Research*, *86*(B4), 2721–2735. https://doi.org/10.1029/JB086iB04p02721

Menzel, M. D., Garrido, C. J., López Sánchez-Vizcaíno, V., Marchesi, C., Hidas, K., Escayola, M. P., & Delgado Huertas, A. (2018). Carbonation of mantle peridotite by CO2-rich fluids: The formation of listvenites in the advocate ophiolite complex (Newfoundland, Canada). *Lithos*, *323*, 238–261. https://doi.org/10.1016/J.LITHOS.2018.06.001

Menzel, M. D., Urai, J. L., de Obeso, J. C., Kotowski, A., Manning, C. E., Kelemen, P. B., et al. (2020). Brittle deformation of carbonated peridotite—Insights from listvenites of the Samail ophiolite (Oman Drilling Project Hole BT1B). *Journal of Geophysical Research: Solid Earth*, *125*(10). https://doi.org/10.1029/2020JB020199

Monnier, C., Girardeau, J., Le Mée, L., & Polvé, M. (2006). Along-ridge petrological segmentation of the mantle in the Oman ophiolite. *Geochemistry, Geophysics, Geosystems*, *7*(11). https://doi.org/10.1029/2006GC001320

Nasir, S., Al-Sayigh, A. R., Al Harthy, A., Al-Khirbash, S., Al-Jaaidi, O., Musllam, A., et al. (2007). Mineralogical and geochemical characterization of listwaenite from the Semail Ophiolite, Oman. *Chemie Der Erde - Geochemistry*, *67*(3), 213–228. https://doi.org/10.1016/j.chemer.2005.01.003

Noël, J., Godard, M., Oliot, E., Martinez, I., Williams, M., Boudier, F., et al. (2018). Evidence of polygenetic carbon trapping in the Oman Ophiolite: Petro-structural, geochemical, and carbon and oxygen isotope study of the Wadi Dima harzburgite-hosted carbonates (Wadi Tayin massif, Sultanate of Oman). *Lithos*, *323*, 218–237. https://doi.org/10.1016/J.LITHOS.2018.08.020

Paulick, H., Bach, W., Godard, M., De Hoog, J. C. M., Suhr, G., & Harvey, J. (2006). Geochemistry of abyssal peridotites (Mid-Atlantic Ridge, 15°20′N, ODP Leg 209): Implications for fluid/rock interaction in slow spreading environments. *Chemical Geology*, *234*(3–4), 179–210. https://doi.org/10.1016/j.chemgeo.2006.04.011

Prigent, C., Agard, P., Guillot, S., Godard, M., & Dubacq, B. (2018). Mantle wedge (De) formation during subduction infancy: Evidence from the base of the Semail Ophiolitic Mantle. *Journal of Petrology*, *59*(11), 2061–2092. https://doi.org/10.1093/petrology/egy090

Quesnel, B., Boulvais, P., Gautier, P., Cathelineau, M., John, C. M., Dierick, M., et al. (2016). Paired stable isotopes (O, C) and clumped isotope thermometry of magnesite and silica veins in the New Caledonia Peridotite Nappe. *Geochimica et Cosmochimica Acta*, *183*, 234–249. https://doi.org/10.1016/j.gca.2016.03.021

Rioux, M., Bowring, S., Kelemen, P. B., Gordon, S., Miller, R., & Dudás, F. (2013). Tectonic development of the Samail ophiolite: High-precision U-Pb zircon geochronology and Sm-Nd isotopic constraints on crustal growth and emplacement. *Journal of Geophysical Research: Solid Earth*, *118*(5), 2085–2101. https://doi.org/10.1002/jgrb.50139

Rioux, M., Garber, J., Bauer, A., Bowring, S., Searle, M. P., Kelemen, P. B., & Hacker, B. (2016). Synchronous formation of the metamorphic sole and igneous crust of the Semail ophiolite: New constraints on the tectonic evolution during ophiolite formation from high-precision U–Pb zircon geochronology. *Earth and Planetary Science Letters*, *451*, 185–195. https://doi.org/10.1016/j.epsl.2016.06.051

Scharf, A., Mattern, F., Bolhar, R., Bailey, C. M., & Ring, U. (2020). U-Pb dating of postobductional carbonate veins in listwaenite of the Oman Mountains near Fanja. *Presented at Proceedings of the International Conference on Ophiolites and the Oceanic Lithosphere: Results of the Oman Drilling Project and Related Research*. Sultan Qaboos University, Oman.

Schwarzenbach, E. M., Früh-Green, G. L., Bernasconi, S. M., Alt, J. C., & Plas, A. (2013). Serpentinization and carbon sequestration: A study of two ancient peridotite-hosted hydrothermal systems. *Chemical Geology*, *351*, 115–133. https://doi.org/10.1016/j.chemgeo.2013.05.016

Schwarzenbach, E. M., Gill, B. C., Gazel, E., & Madrigal, P. (2016). Sulfur and carbon geochemistry of the Santa Elena peridotites: Comparing oceanic and continental processes during peridotite alteration. *Lithos*, *252–253*, 92–108. https://doi.org/10.1016/j.lithos.2016.02.017

Searle, M. P., & Cox, J. (2002). Subduction zone metamorphism during formation and emplacement of the Semail ophiolite in the Oman Mountains. *Geological Magazine*, *139*(3), 241–255. https://doi.org/10.1017/S0016756802006532

Searle, M. P., & Malpas, J. (1980). Structure and metamorphism of rocks beneath the Semail ophiolite of Oman and their significance in ophiolite obduction. *Transactions of the Royal Society of Edinburgh Earth Sciences*, *71*(4), 247–262. https://doi.org/10.1017/S0263593300013614

Searle, M. P., Waters, D. J., Martin, H. N., & Rex, D. C. (1994). Structure and metamorphism of blueschist-eclogite facies rocks from the northeastern Oman Mountains. *Journal of the Geological Society*, *151*(3), 555–576. https://doi.org/10.1144/gsjgs.151.3.0555

Soret, M., Agard, P., Dubacq, B., Plunder, A., & Yamato, P. (2017). Petrological evidence for stepwise accretion of metamorphic soles during subduction infancy (Semail ophiolite, Oman and UAE). *Journal of Metamorphic Geology*, *35*(9), 1051–1080. https://doi.org/10.1111/jmg.12267

Stanger, G. (1985). Silicified serpentinite in the Semail nappe of Oman. *Lithos*, *18*, 13–22. https://doi.org/10.1016/0024-4937(85)90003-9

Stewart, E. M., & Ague, J. J. (2020). Pervasive subduction zone devolatilization recycles CO2 into the forearc. *Nature Communications*, *11*(1), 1–8. https://doi.org/10.1038/s41467-020-19993-2

Tibi, R., Wiens, D. A., & Yuan, X. (2008). Seismic evidence for widespread serpentinized forearc mantle along the Mariana convergence margin. *Geophysical Research Letters*, *35*(13), 267–270. https://doi.org/10.1029/2008GL034163

Tsuji, Y., Nakajima, J., & Hasegawa, A. (2008). Tomographic evidence for hydrated oceanic crust of the Pacific slab beneath northeastern Japan: Implications for water transportation in subduction zones. *Geophysical Research Letters*, *35*(14), 1–5. https://doi.org/10.1029/2008GL034461

Villey, M., Le Metour, J., & de Gramont, X. (1986). *Geological Map of Fanjah*. Ministry of Petroleum and Minerals, Directorate General of Minerals. Sultanate of Oman.

Weis, D., Kieffer, B., Maerschalk, C., Barling, J., De Jong, J., Williams, G. A., et al. (2006). High-precision isotopic characterization of USGS reference materials by TIMS and MC-ICP-MS. *Geochemistry, Geophysics, Geosystems*, *7*(8). https://doi.org/10.1029/2006GC001283

Weyhenmeyer, C. E. (2000). *Origin and evolution of groundwater in the alluvial aquifer of the Eastern Batinah Coastal Plain, Sultanate of Oman: A hydrogeochemical approach* (PhD thesis). Universität Bern.

Wilde, A., Simpson, L., & Hanna, S. (2002). Preliminary study of tertiary hydrothermal alteration and platinum deposition in the Oman ophiolite. *Journal of the Virtual Explorer*, *6*, 7–13.

Yoshikawa, M., Python, M., Tamura, A., Arai, S., Takazawa, E., Shibata, T., et al. (2015). Melt extraction and metasomatism recorded in basal peridotites above the metamorphic sole of the northern Fizh massif, Oman ophiolite. *Tectonophysics*, *650*, 53–64. https://doi.org/10.1016/j.tecto.2014.12.004

Zeko, D. (2021). *Carbonation of the Oman ophiolite during subduction and emplacement*. University of British, Columbia.